Environmental Earth Sciences (2019) 78:36
https://doi.org/10.1007/s12665-018-8018-x

THEMATIC ISSUE

Inland impacts of atmospheric river and tropical cyclone extremes on nitrate transport and stable isotope measurements

A. Husic[1] · J. Fox[2] · E. Adams[2] · J. Backus[3] · E. Pollock[4] · W. Ford[5] · C. Agouridis[5]

Received: 30 June 2018 / Accepted: 19 December 2018

Abstract

Atmospheric rivers and tropical cyclones originate in the tropics and can transport high rainfall amounts to inland temperate regions. The purpose of this study was to investigate the response of nitrate (NO_3^-) pathways, concentration peaks, and stable isotope ($\delta^{15}N_{NO3}$, $\delta^{18}O_{NO3}$, $\delta^{2}H_{H2O}$, $\delta^{18}O_{H2O}$, and $\delta^{13}C_{DIC}$) measurements to these extreme events. A tropical cyclone and atmospheric river produced the number one and four ranked events in 2017, respectively, at a Kentucky USA watershed characterized by mature karst topography. Hydrologic responses from the two events were different due to rainfall characteristics with the tropical cyclone producing a steeper rising limb of the spring hydrograph and greater runoff generation to the surface stream compared to the atmospheric river. Local minima and maxima of specific conductance, $\delta^{2}H_{H2O}$, $\delta^{18}O_{H2O}$, and $\delta^{13}C_{DIC}$ coincided with hydrograph peaks for both events. Minima and maxima of NO_3^-, $\delta^{15}N_{NO3}$, $\delta^{18}O_{NO3}$, and temperature lagged behind the hydrograph peak for both events, and the values continued to be impacted by diffuse recharge during hydrograph recession. Quick-flow pathways accounted for less than 20% of the total NO_3^- yield, while intermediate (30%) and slow-flow (50%) pathways composed the remaining load. However, hydrograph separation into quick-, intermediate-, and slow-flow pathways was not able to predict the timing of NO_3^- concentration peaks. Rather, the intermediate-flow pathway is conceptualized to experience a shift in porosity, associated with a change from epikarst macropores and fissures to soil micropores, with the arrival of water from the latter component likely causing peak NO_3^- concentration at the spring. Our results suggest that a more discretized conceptual model of pathways may be needed to predict peak nutrient concentration in rivers draining karst topography.

Keywords Karst · Nitrate · Pathways · Contaminant transport · Extreme events

Introduction

The inland trajectory of atmospheric river and tropical cyclone extreme events can impact the hydrologic cycle thousands of kilometers from coastal landfall (Moore et al. 2012; Lavers and Villarini 2013). Atmospheric rivers are narrow bands of transported moisture that carry water vapor from the tropics to temperate regions (Rutz et al. 2014). Tropical cyclones also originate in the tropics, and carry moisture via high-speed cyclonic winds to sub-tropic and temperate regions (Knight and Davis 2009). Tropical storms generate highly dangerous conditions upon making landfall, such as endangering human life and flooding manmade infrastructure (Lavers et al. 2012; Ralph and Dettinger 2012). In addition, their effects are felt far inland where storm remnants can drive local hydrology. For example, in the southeastern USA, atmospheric rivers can account for over one-third of total annual rainfall (Lavers and Villarini

This article is a part of Topical Collection in environmental earth sciences on characterization, modeling, and remediation of karst in a changing environment, guest edited by Zexuan Xu, Nicolas Massei, Ingrid Padilla, Andrew Hartmann, and Bill Hu.

✉ A. Husic
ahusic@ku.edu

[1] Department of Civil, Environmental, and Architectural Engineering, University of Kansas, Lawrence, USA

[2] Department of Civil Engineering, University of Kentucky, Lexington, USA

[3] Kentucky Geological Survey, University of Kentucky, Lexington, USA

[4] Stable Isotope Laboratory, University of Arkansas, Fayetteville, USA

[5] Department of Biosystems and Agricultural Engineering, University of Kentucky, Lexington, USA

Published online: 02 January 2019

2013) and tropical cyclones are most likely to produce the largest annual event (Shepherd et al. 2007). The intensity of these extreme events is projected to increase as climate change alters regional hydrology (Lavers and Villarini 2013).

Given the high inland rainfall amounts associated with extremes events, their impact on mobilizing water contaminants is also of question. During rainfall and immediately thereafter, contaminants can be mobilized from surface and subsurface sources via runoff, lateral soil flow, and groundwater flow. Peak contaminant concentrations in river water during or after an event can be detrimental to ecosystems (Cánovas et al. 2008; Jarsjö et al. 2017). Therefore, we are interested in understanding the inland impacts of atmospheric rivers and tropical cyclones on contaminant pathways and concentrations peaks, particularly with respect to NO_3^- contamination.

Nitrate in rivers is of immediate concern as human activities have increased NO_3^- loading to waterways leading to the development of harmful algal blooms and hypoxic zones (Dodds and Smith 2016). Past research provides some hints as to how NO_3^- may be mobilized from pathways during extreme events. Nitrate pathways from the landscape to rivers can include dilute quick flow from runoff, slow flow of groundwater, and concentrated quick flow (Tesoriero et al. 2013; Miller et al. 2017). The timing and relative NO_3^- contribution of these pathways are expected to result in a peak NO_3^- concentration that is delayed ("lagged") relative to the hydrograph peak (Koenig et al. 2017). However, the prevailing nutrient paradigm remains open-ended with questions regarding both the distribution of pathways throughout a basin and the cause of peak concentration timing. The importance of understanding these pathways becomes more apparent as climate change exerts influence on inland hydrology (Al Aamery et al. 2016, 2018) and land management strategies adapt to extreme events (Tomer and Schilling 2009; Lal et al. 2011).

Research tools applied to understand NO_3^- pathways and peaks during extremes include both high-resolution sampling routines and quantitative analysis of pathways. Storm event sampling of water, NO_3^-, and its indicators can help to resolve mobilization from different pathways. In addition, NO_3^- source and fate can be investigated using stable isotopes (i.e., $\delta^{15}N_{NO3}$ and $\delta^{18}O_{NO3}$) (Panno et al. 2001; Katz et al. 2010; Yue et al. 2018). Quantitative analysis of NO_3^- pathways can be assessed using loadograph recession analyses (Mellander et al. 2012; Fenton et al. 2017), whereby inflection points on the recession can be used to quantify pathway contributions of NO_3^- storages zones (Fenton et al. 2017). Assessment of the lag effect corresponding with the relative locations of discharge and concentration peaks can be used to infer causes and pathways of contamination (Koenig et al. 2017). Likewise, water and dissolved inorganic (DIC) isotopic composition can assist in identifying pathways (Lee and Krothe 2001). However, there is a lack of relatively high-frequency data collection of stable isotope measurements during extreme events as the events are, by their nature, infrequent.

The 2017 calendar year brought an unusually high number of atmospheric river and tropical cyclone extremes to inland North America. January and February 2017 brought a string of atmospheric rivers to the contiguous United States (US), and June–November 2017 was one of the most active hurricane seasons on record featuring 17 tropical cyclones in the Atlantic and Caribbean (NHC NOAA 2017). After effects resulted in approximately 1,000 fatalities and damage to infrastructure totaling $300 billion, making 2017 the costliest year on record for natural disasters (NOAA 2017a). While recognizing the distressing impact on human life, we questioned the inland impacts of extreme events on NO_3^- contaminant pathways, stable isotope measurements, and peak concentrations in rivers. As the 2017 extreme events approached Kentucky, USA, our research team carried out an extensive storm sampling plan to understand their impact on mobilizing NO_3^- in a mature karst watershed.

The study objectives were to (1) characterize the inland impacts of extreme events, including their timing, rainfall amounts, intensities, and hydrograph responses for a karst watershed in Kentucky; (2) collect and analyze water-quality and environmental tracer data mobilized by the extreme events; (3) perform hydrograph and loadograph separation analyses for NO_3^- pathways; (4) perform nutrient lag-effect analysis. The objectives provide the structural sub-headings of the "Methods" and "Results and discussion" sections of this paper.

Theoretical background

Both atmospheric rivers and tropical cyclones can produce high rainfall amounts far inland, such as in Kentucky (Fig. 1a). A set of atmospheric rivers, termed the "Maya Express", transports moisture from the eastern tropical Pacific and the Caribbean Sea into the US Midwest and Southeast (Fig. 1b) (Moore et al. 2012; Debbage et al. 2017). During the wet season, which historically runs between December and May in Kentucky (Husic 2018), southerly atmospheric rivers can account for 30–50% of rainfall in the region (Lavers and Villarini 2013). The term 'tropical cyclone' refers to low-pressure, rotating storm systems formed in the tropics and characterized by high wind speeds and rainfall intensities (Larson et al. 2005). Tropical cyclones that originate in the mid-Atlantic Ocean often make landfall in the Caribbean and Southeastern USA and can have trajectories that reach far inland (see Fig. 1c). In terms of watershed hydrology for

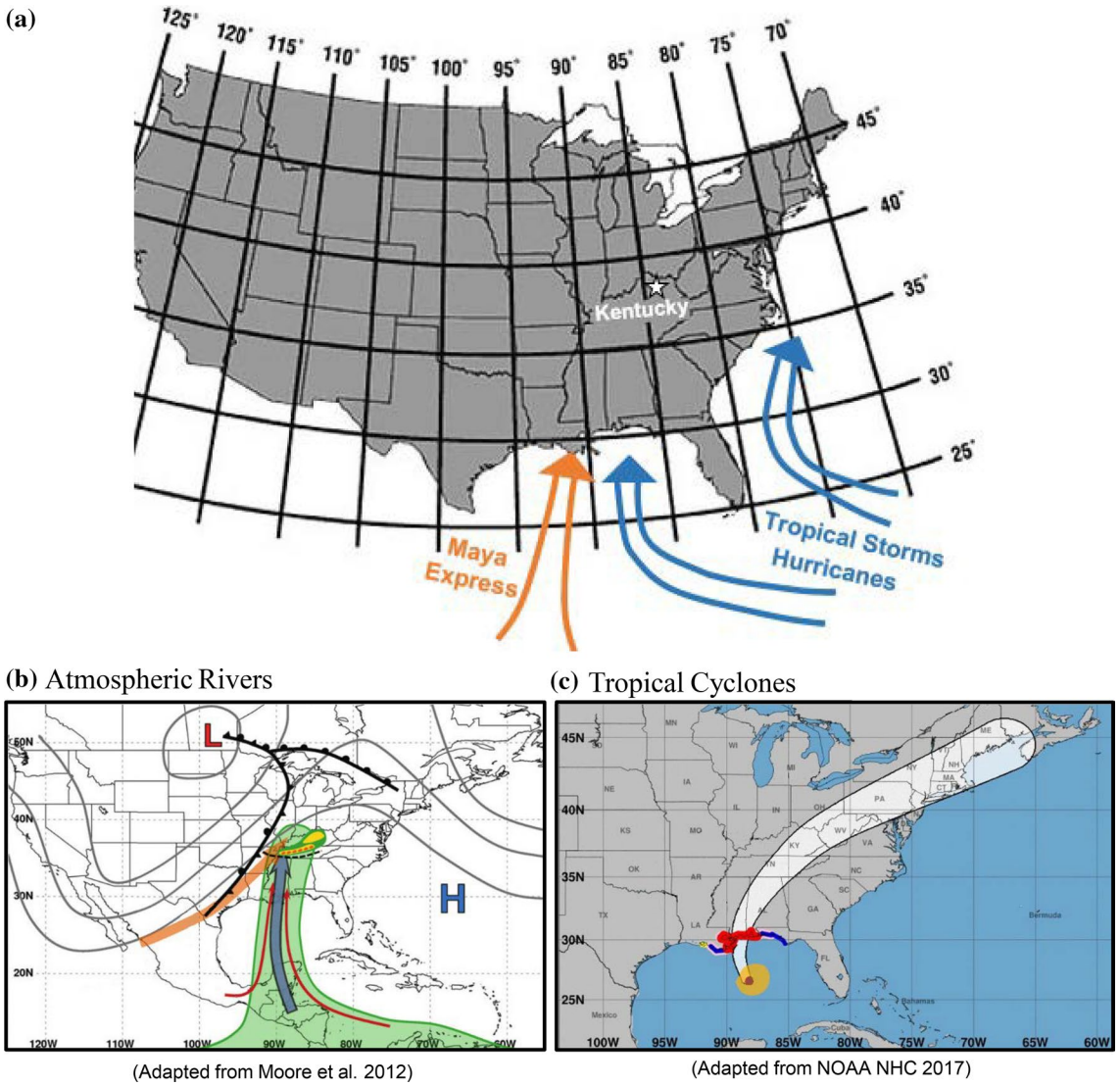

Fig. 1 **a** Locations and names of extreme events falling on the conterminous United States. Atmospheric rivers, such as the Maya Express (orange arrow), and tropical cyclones, such as hurricanes and tropical storms (blue arrows), make coastal landfall and can travel far inland. The white star represents the study region located within Kentucky. **b** Trajectory of the Maya Express (Moore et al. 2012). Surface fronts are shown in their standard frontal notation. The orange line represents a stream of dry mid-level air and the blue line represents the atmospheric river. Red lines and the green shading around the atmospheric river denote streamlines above the atmospheric boundary layer and areas of high-water vapor. **c** Trajectory of an inland tropical cyclone (NHC NOAA 2017). The light orange shading represents areas of tropical-level winds. Red and blue colors indicate hurricane and tropical storm warnings, respectively. The white cone represents probable path of the storm center

inland regions of North America, the seasonality of these extremes allows us to investigate atmospheric rivers and tropical cyclones as two separate classifications of extreme rainfall events. The mid- to late-winter atmospheric rivers bring high rainfall, distributed over days, upon wet soils, while the late-summer and early fall hurricanes bring extreme rainfall upon dry soils. In this manner, extreme events in the central Kentucky region may be characterized by behavior that falls between that of atmospheric rivers and tropical cyclones.

Pathways of nitrogen (N) transport include a mixture of quick-flow, intermediate-, and slow-flow pathways distributed across a storm event. A more-refined view of pathways is conceptualized by considering karst-dominated watersheds typical of Kentucky (see Fig. 2a). The Kentucky karst region is characterized by gently rolling terrain caused by the dissolution of limestone, which in turn produces sinkholes, sinking streams, springs, and conduits (Fig. 2b; Phillips et al. 2004). In highly karstified systems, direct quick-flow recharge into conduit systems dominates the early

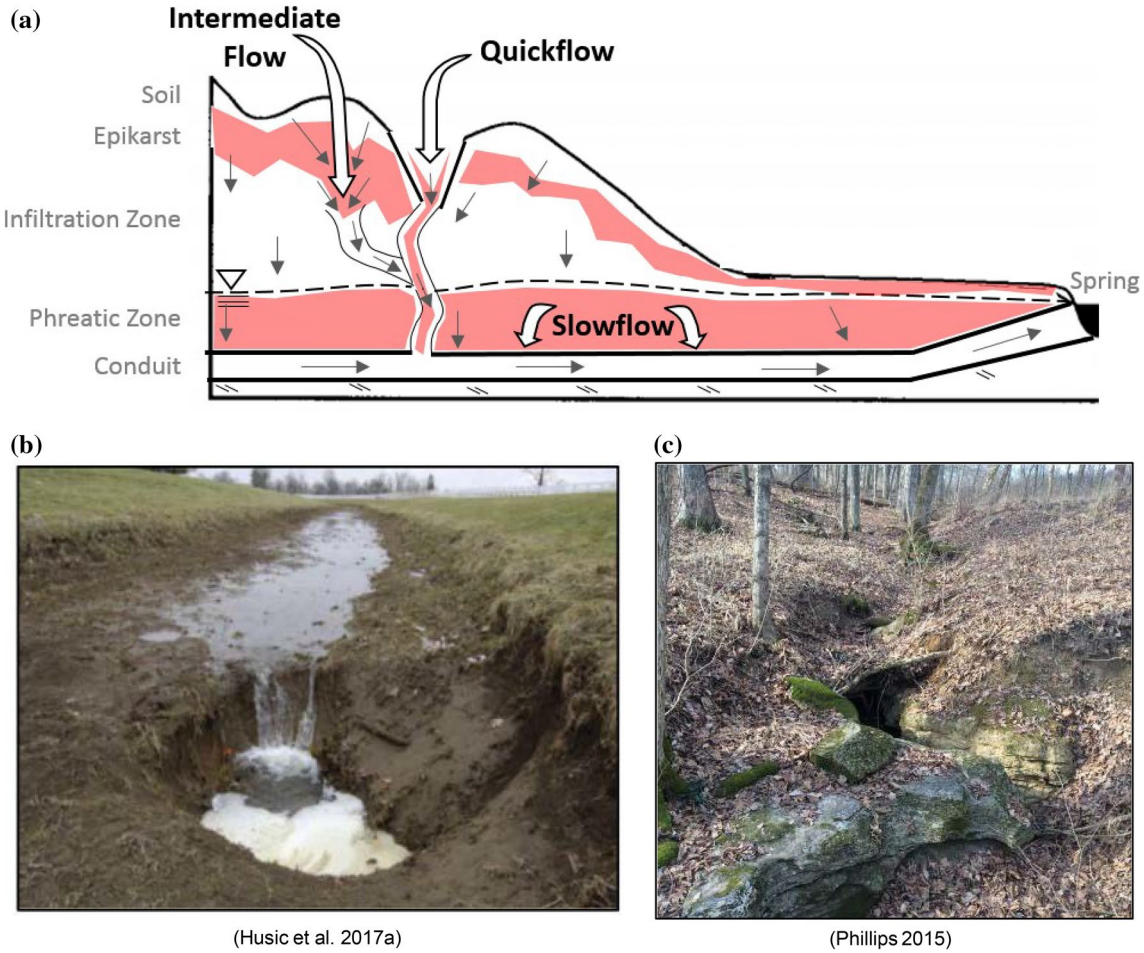

Fig. 2 **a** Diagram showing quick, intermediate (epikarst and soil), and slow (phreatic) flow pathways. **b** A swallet in Cane Run Creek, Kentucky (Husic et al. 2017a). **c** Surficial epikarst features in Bowman's Bend of the Kentucky River (Phillips 2015)

hydrograph response (Geyer et al. 2007). Diffuse recharge follows soil, epikarst, and phreatic zone pathways where storage volumes are several orders of magnitude greater than that of quick-flow pathways and have the potential to retain N (Williams 2008) (see Fig. 2c for epikarst example). We conceptualize diffuse recharge as two pathways, including intermediate (following soil pores and epikarst fractures) and slow (following the phreatic rock matrix) flow pathways (Fig. 2a). Intermediate pathway storages, such as soil and epikarst, provide the potential for high N accumulation and subsequent leaching (Tzoraki and Nikolaidis 2007), which may deliver highly concentrated NO_3^-. Slow-flow pathways reflect phreatic storage sustained by Darcian groundwater flow from stored volumes in the aquifer bedrock matrix (Vesper and White 2004).

These pathways mobilize and deliver both dilute and concentrated NO_3^- to rivers. Identifying variability in NO_3^- concentration during storm conditions requires relatively high-frequency sampling as lower sampling rates may miss changes in source contribution. For the watershed scale, a lagged N concentration peak involves a sequence of initially dilute quick flow followed by concentrated intermediate flow and subsequent slow flow from groundwater stores (Miller et al. 2017). As the dilute quick flow recedes and gives way to the intermediate- and slow-flow pathways, a peak NO_3^- concentration is expected. The long-term NO_3^- concentration is then associated with slow pathways that sustain baseflow (Burns et al. 2016). While nutrient concentrations may be impacted by biogeochemical activity during low flows (Moatar et al. 2017), we expect that, during high flows in a karst watershed, NO_3^- concentrations will be dominated by hydrological pathways. The dilution/concentration dynamics discussed in this section relate primarily to dissolved nutrient phases, whereas particulate nutrients, such as phosphorous, are associated more closely with quick flow (Jarvie et al. 2014).

As atmospheric river and tropical cyclone extremes approached Kentucky, a sampling plan was carried out to investigate how extreme events mobilize pathways, impact

stable isotope measurements, and produce peak N concentrations. This plan is described below.

Study site and materials

The Cane Run watershed (96 km^2) and Royal Spring groundwater basin (58 km^2) are located in the Inner Bluegrass Region of Kentucky (Fig. 3), approximately 1000 km from the Gulf of Mexico where atmospheric rivers and tropical cyclones made landfall in 2017. The study watershed is characterized by rolling hills and mild relief (Paylor and Currens 2004). This topography makes the land surface suitable for agricultural use, and much of it is horse farm pasture (UKCAFE 2011). The spring basin is underlain by Lexington Limestone of the Middle Ordovician period (Cressman and Peterson 1986). The karst of this region is characterized as telogenetic, indicating the previous compaction and burial by overlying sediment, and much of the aquifer recharge is through discrete karst fractures, sometimes to the exclusion of other fluvial features (Phillips et al. 2004). The groundwater flow follows a series of en-echelon minor faults and joints trending from the southeast to the northwest (Drahovzal et al. 1992). Surface and subsurface flow pathways are highly connected, with over 50 swallets identified in the field (Fig. 3) (Paylor and Currens 2004; Husic et al. 2017a). These swallets are situated in silt loam and silty clay loam formed from the residue of weathered phosphatic limestone (USDA 1993). Tributary recharge to the primary creek channel is abstracted by swallets to a trunk conduit 20 m below the earth surface (see "conduit conveyance zone" in Fig. 3). Flow abstraction in Cane Run is so prevalent that the primary creek flows less than 20% of the year, only becoming active during moderate-to-intense hydrologic activity (Husic et al. 2017a). The mean discharge of the primary spring draining the aquifer, Royal Spring (243 m.a.s.l.), is 0.67 $m^3\ s^{-1}$. The basin has been studied by the Kentucky Geological Survey and the University of Kentucky for the past 40 years (Spangler 1982; Thrailkill et al. 1991; Taylor 1992; Paylor and Currens 2004; Zhu et al. 2011; Husic et al. 2017a, b).

Three sampling stations were located in the basin, including the surface stream that recharges the karst aquifer (Cane Run Creek), the midpoint of the subsurface phreatic conduit (Phreatic Conduit), and the primary karst spring (Royal Spring) (Fig. 3). Groundwater wells were drilled at the "Phreatic Conduit" station to sample from within the submerged conduit near its longitudinal midpoint (Zhu et al. 2011; Husic et al. 2017a). The conduit was sampled with a deep well pump (Hallmark Industries MA0414X-7) submerged directly into the primary flow path. The United States Geological Survey (USGS) operates a gage at Royal Spring (USGS 03288110) where discharge was recorded and grab samples were collected. The Cane Run Creek surface

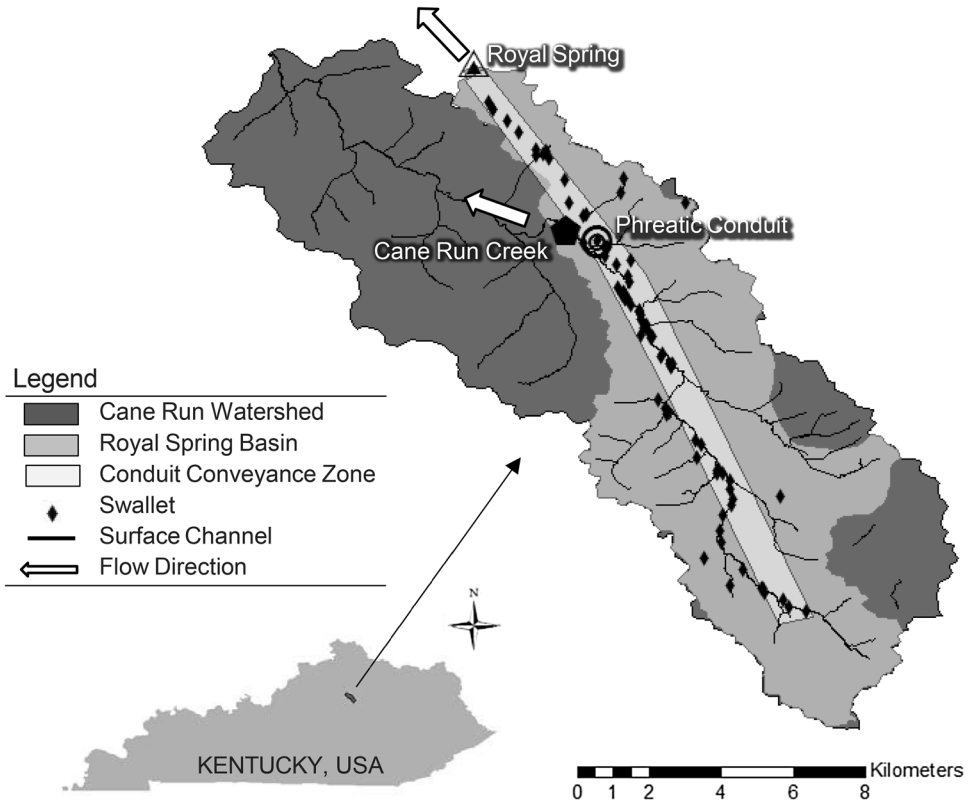

Fig. 3 A map of Cane Run Watershed and Royal Spring Groundwater Basin, indicating the locations of the three sampling sites (Royal Spring—spring water, Phreatic Conduit—ground water, and Cane Run Creek—surface water), the conduit conveyance zone, swallets, surface channels, and the flow directions for surface and subsurface drainages

station was sampled using a Teledyne ISCO 6712 pump sampler affixed to the streambed. The Cane Run Creek station did not have an operational gage during the period of this study, so streamflow was monitored 9 km upstream at Citation Boulevard (USGS 03288180). A previous relationship, developed for discharge between Cane Run Creek (Q_{CRC}) and Citation Boulevard (Q_{BLVD}), showed general agreement between the two sites ($Q_{CRC} = 1.12 \times Q_{BLVD} - 0.65$, and $R^2 = 0.73$; Husic 2015), and provided confidence in the use of Citation Boulevard to describe surface flow conditions. Rainfall data were available from the Bluegrass Airport (NOAA ID: USW00093820).

Methods

Characterizing extreme events and their hydrographs

Storm events were characterized based on the meteorological conditions responsible for rainfall. During 2017, four events, of the 70 that occurred (Fig. 4), were characterized as extreme events (i.e., the 95th percentile; Gao et al. 2012). Two of these events were the subjects of this study: one produced by an atmospheric river in late February 2017 and another by a tropical cyclone in early October 2017. The atmospheric river originated in the Gulf of Mexico, joined a cold front from the Great Plains, and produced the fourth largest rainfall event in the study watershed (Fig. 4). The tropical cyclone, known as "Hurricane Nate", originated from a broad area of low pressure over the southwestern Caribbean. The inland impact of Hurricane Nate produced the largest rainfall event in 2017 for the study site (Fig. 4). Events were ranked as the maximum 3-day sums of recorded precipitation.

Antecedent conditions of the watershed were also of interest to characterizing flow hydrographs. Storms were sampled based on (1) the expected rainfall intensity (so as to create a significant response at the three sampling locations), and (2) antecedent spring conditions (lower initial spring flow allowed for the attribution of more flow to storm water rather than pre-event water). Hydrograph shapes were then compared across storm events as the steepness and slope(s) of the rising and falling limb(s) can coincide with changes in quick and diffuse flow contributions, respectively (Geyer et al. 2008).

Water-quality and environmental tracer data collection

Specific conductance, temperature, NO_3^-, $\delta^{15}N_{NO3}$, $\delta^{18}O_{NO3}$, $\delta^{2}H_{H2O}$, $\delta^{18}O_{H2O}$, and $\delta^{13}C_{DIC}$ samples were collected to show the timing and pathways of contaminants. The temporal sampling strategy included high-frequency data collection during various points of a storm hydrograph, including pre-event baseflow, rising limb flow, peak discharge, and the beginning, middle, and end of storm recession. Water samples were collected directly from the mouth of the spring into sterile 1 L jars (I-Chem 312-0950BPC). At the creek site, if the water level was sufficiently low, grab samples were collected directly from the stream. Otherwise, such as during high-water conditions, water was pumped from the creek bottom using the automated sampler. At the conduit site, the pump extracted water directly from within the conduit into sterile 1 L jars. If time did not permit installation of the pump before an event began, samples were collected using a double-check valve bailer (AMS 61844).

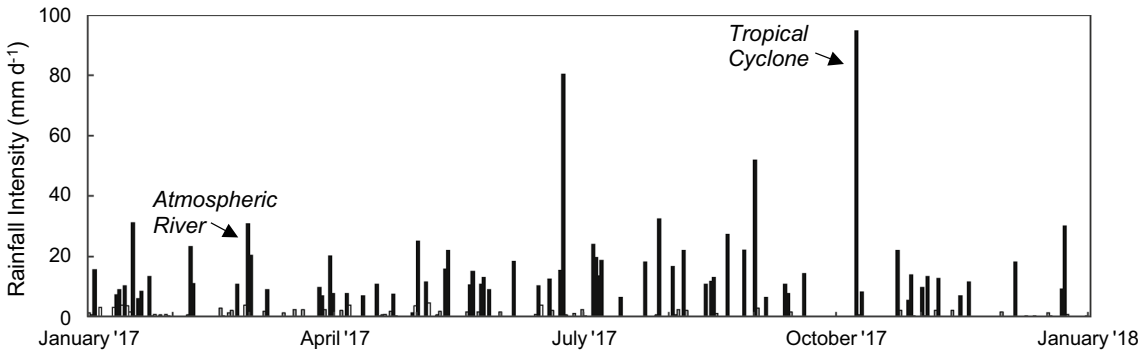

Extreme Event	Date	Season	Rank (in 2017)	Precipitation (mm)
Atmospheric River	February 28, 2017	Winter/ Spring	4	54.9
Tropical Cyclone	October 8, 2017	Fall	1	103.4

Fig. 4 Rainfall intensity for the 2017 calendar year and the timing of two sampled extreme events. Total annual rainfall was 1249 mm. Rank was determined by the 3-day event precipitation total

Water depth in a well directly intersecting the conduit was measured with a well-level indicator (Slope 113583). A multi-parameter probe (Horiba U-10) was used to record temperature and specific conductance data. For each set of samples, the time elapsed between collection from the first site to the last site was kept to a minimum (< 1 h).

The Kentucky Geological Survey (KGS) laboratory analyzed NO_3^- samples following US EPA Method 300.0. The analysis was performed using a Dionex ICS-3000 Ion Chromatography System featuring a carbonate–bicarbonate eluent generator and Dionex AS4A analytical column. Retention time was used to identify the NO_3^- anion, and peak areas were compared to calibration curves generated from known standards. Duplicate field samples of NO_3^- showed a little variability ($n = 8$, ± 0.07 mg N L^{-1}). Likewise, lab duplicates also showed a little variability ($n = 49$, ± 0.02 mg N L^{-1}). No lab, field, or equipment blanks registered above the method detection limit (MDL).

Samples for $\delta^{15}N_{NO3}$, $\delta^{18}O_{NO3}$, $\delta^{2}H_{H2O}$, $\delta^{18}O_{H2O}$, and $\delta^{13}C_{DIC}$ analyses were extracted in the field from the bulk 1 L jars using clean 60 mL syringes and passed through 0.45 µm syringe filters (Whatman 6780-2504) into sterile 40 mL borosilicate vials (I-Chem TB36-0040). Each borosilicate vial came with a permeable 1.5 mm septum; however, the use of permeable septum can contaminate $\delta^{13}C_{DIC}$ values, so vials for dissolved inorganic carbon (DIC) analysis were amended with an additional thick butyl rubber septum (St-Jean 2003). Samples were stored in a refrigerated environment without the use of preservatives for less than a week before delivery to the University of Arkansas Stable Isotope Lab (UASIL) for analysis. The isotopic ratio (δ) is reported in units of per mille (‰) and represents the relative abundance of heavy-to-light isotopes in a sample and is calculated as follows:

$$\delta = \left(\frac{R_{\text{sample}} - R_{\text{standard}}}{R_{\text{standard}}} \right) \times 1000, \quad (1)$$

where R is the ratio of the abundance of the heavy-to-light isotopes, sample is the field sample, and standard is the reference standard of the known isotope ratio. The references used for the analysis of N, C, O, and H isotopes were AIR, Vienna Pee Dee Belemnite (VPDB), and Vienna Standard Ocean Water (VSMOW), respectively. Isotope data for NO_3^- were produced using the bacterial denitrifier method with a Thermo Scientific GasBench II (Sigman et al. 2001; Casciotti et al. 2002). Isotope data for H_2O were produced using high-temperature pyrolysis with a Thermo Scientific TCEA with modified reverse-flow set-up (Gehre et al. 2004). Isotope data for DIC were produced by converting DIC to CO_2 through the use of a phosphoric acid with a Thermo Scientific GasBench II (Knierim et al. 2013). The isotopic reference materials for NO_3^- were USGS32 ($\delta^{15}N_{NO3} = +180$‰), USGS34 ($\delta^{15}N_{NO3} = -1.8$‰, $\delta^{18}O_{NO3} = -27.9$‰), and USGS35 ($\delta^{18}O_{NO3} = +57.5$‰). Average standard deviations for the NO_3^- isotopic standards were 2.03‰ for USGS32 for $\delta^{15}N$; 0.34 and 0.70‰ for USGS34 for $\delta^{15}N$ and $\delta^{18}O$, respectively; and 1.00‰ for USGS35 for $\delta^{18}O$. Duplicates of $\delta^{15}N_{NO3}$ and $\delta^{18}O_{NO3}$ ($n = 5$) had standard deviations of ± 0.28‰ and ± 0.45‰, respectively. The isotopic reference material for DIC was NBS 19 ($\delta^{13}C = +1.95$‰) and two house standards (UASIL 22, UASIL23), and average standard deviation for the standards was ± 0.09‰. Duplicates of $\delta^{13}C_{DIC}$ ($n = 5$) had a standard deviation of ± 0.37‰. Water hydrogen and oxygen stable isotope samples were normalized to VSMOW using three isotopically distinct standards (USGS47, UASIL_L, and UASIL_R) with a precision of ± 1.0‰ and ± 0.2‰, for H and O, respectively. All detection was accomplished through interfacing with a Thermo Scientific Delta Plus or Delta V Advantage IRMS.

Hydrograph and loadograph separation analyses

The receding limb of the spring hydrograph can be conceptualized as the draining of multiple reservoirs with varying porosities, hydraulic conductivities, and storage volumes. The exponential form of recession is the most common method used in the analysis of karst springs (Fiorillo 2014). We construct a composite exponential recession to represent the drainage of multiple reservoirs. Each linear segment of the log plot of spring discharge represents a different reservoir and each segment was identified graphically using the constant slope method (Fiorillo 2014). In this study, three segments were identified and characterized quick, intermediate (epikarst and soil), and slow (phreatic) flow water. The quick and intermediate flows were separated by the first inflection point in the recession, while the intermediate and slow flows were separated by the second inflection point.

Loadograph recession was coupled with the hydrograph recession analysis and NO_3^- loads were quantified for each pathway (Fenton et al. 2017). Nitrate load is the product of spring discharge and NO_3^- concentration. While discharge data were available continuously (every 15 min), NO_3^- data were discretely collected. To develop a continuous loadograph, NO_3^- concentration at the spring was estimated by interpolating between discretely collected samples. The sample collection design for this study justified interpolation as the highest frequency data collection occurred during periods of greatest change at the spring. Thus, the total NO_3^- yield was estimated by integrating under the loadograph over the course of the event. The inflection points identified in the hydrograph analysis were superimposed onto the NO_3^- loadograph (Fenton et al. 2017). Each pathway comprises an area under the loadograph and, by integrating that area, a total contribution of that pathway can be estimated (Mellander et al. 2012). The pathways and

methodology used in this study were similar to the other karst studies such as Fenton et al. (2017), who used continuous sensor N data to estimate conduit, large-, medium-, and small-fissure pathway contributions.

Nutrient lag effect in rivers

Streams act as integrators of upstream sources and processes, and their pathways impact the timing and magnitude of solute transport (Koenig et al. 2017). We assessed the nutrient lag effect at Royal Spring by investigating the temporal changes in the water-quality and environmental tracer data. Furthermore, we compared these temporal trends with respect to the discharge by each pathway as estimated from the composite hydrograph separation. To identify the nutrient lag effect, the timing of peak NO_3^- concentration was compared to the timing of maximum flow contribution from quick, intermediate, and slow flows. The extent to which water-quality or environmental tracer data lag was used to infer dominant storage and transfer processes impacting contaminant concentrations at karst springs.

We anticipated utilizing chemograph separation via environmental isotopes as an additional measure of nutrient loading and lag; however, the extreme events in this study caused non-stationarity in the source end-members, thus, violating a core assumption of unmixing analysis. This point is explored further in the discussion.

Results and discussion

Characterizing extreme events and their hydrographs

The 2017 calendar year was wet (1249 mm) compared to the historical average annual precipitation of 1170 (±200) mm (Fig. 4). It was also a year characterized by the landfall of many extreme events and the migration of these events far inland from coastal landfall. The four largest events (in order of occurrence) were an atmospheric river in February (sampled), Tropical Storm Cindy in June (not sampled), a thunderstorm in July (not sampled), and Hurricane Nate in October (sampled). The four storms together delivered 25% of the annual rainfall.

The atmospheric river occurring in February 2017 provided 54.9 mm of rainfall over the course of 3 days (Fig. 5). Rainfall on the first day of the event caused a steep increase in spring discharge (to 2 $m^3\ s^{-1}$) followed by a second day of rain and another increase in discharge (to 4 $m^3\ s^{-1}$). Though the event occurred in the late winter/early spring, the initial discharge at Royal Spring was relatively low for this season which highlights the flushing of new water through the system. Discharge in the surface stream initially rose to 4 $m^3\ s^{-1}$ on the first day of rainfall and nearly returned to baseflow conditions, but a second day of rainfall caused another peak in stream discharge of 6 $m^3\ s^{-1}$.

The tropical cyclone in October 2017 was the largest event of the calendar year with the bulk of precipitation falling in a single day (Fig. 5). Pre-event conditions were extremely dry with a low-flow period of 70 days, many of which had no flow at all, preceding the event. The fall season typically receives the least amount of rainfall in Kentucky (NOAA 2017b), so many extreme events of this type are expected to make landfall on dry soil and baseflow conditions. Therefore, the 103.4 mm of rainfall during the year's largest event produced a smaller peak spring discharge (Q_{max} = 2 $m^3\ s^{-1}$) than the fourth largest event (i.e., the atmospheric river), which delivered 54.9 mm of rainfall (Q_{max} = 4 $m^3\ s^{-1}$). Further, the flow in the creek, during the tropical cyclone, approached 12 $m^3\ s^{-1}$ (nearly double the maximum stream discharge for the atmospheric river), but much of this flow simply overtopped in-stream swallets and exited the system via the surface stream.

We find few, if any, studies that directly link hydrologic responses in karst systems to multiple types of extreme events including atmospheric rivers and tropical cyclones. Therefore, we did not have the past literature studies for direct comparison to our results. However, our results of tropical extremes impacting inland karst tend to be corroborated by the study of other karst watersheds with highly connected surface and subsurface flow paths (Martin and Dean 2001; Geyer et al. 2007; Herman et al. 2008; Hartmann et al. 2014). Similar to the work of others, our results showed that the distribution of rainfall was important to the structure of the spring hydrograph (Fiorillo 2014). We observed a larger loss of water to the surface creek, as runoff, with increased rainfall intensity. This loss could likely be associated with an exceedance of the hydrologic carrying capacity of recharging quick-flow features (e.g., sinkholes and swallets). This idea is corroborated by a study in Pennsylvania USA that noted a non-linear relationship between rainfall and spring discharge during extreme precipitation activity (Herman et al. 2008). Thus, it appears that karst springs may be limited to the immediate hydrologic impact of extreme events as more water is lost, with increasing rainfall activity, to surface drainage pathways. The extent to which this holds true for other karst systems is influenced by system-dependent hydrogeologic factors such as meteorological patterns, the extent of karstification, and genetic carbonate structure (eogenetic vs telogenetic) (Florea and Vacher 2006). The implication of this result is that flow and contaminants in surface streams of telogenetic karst systems should be closely monitored during extreme events, even in systems where the subsurface drains the vast majority of flow from the watershed

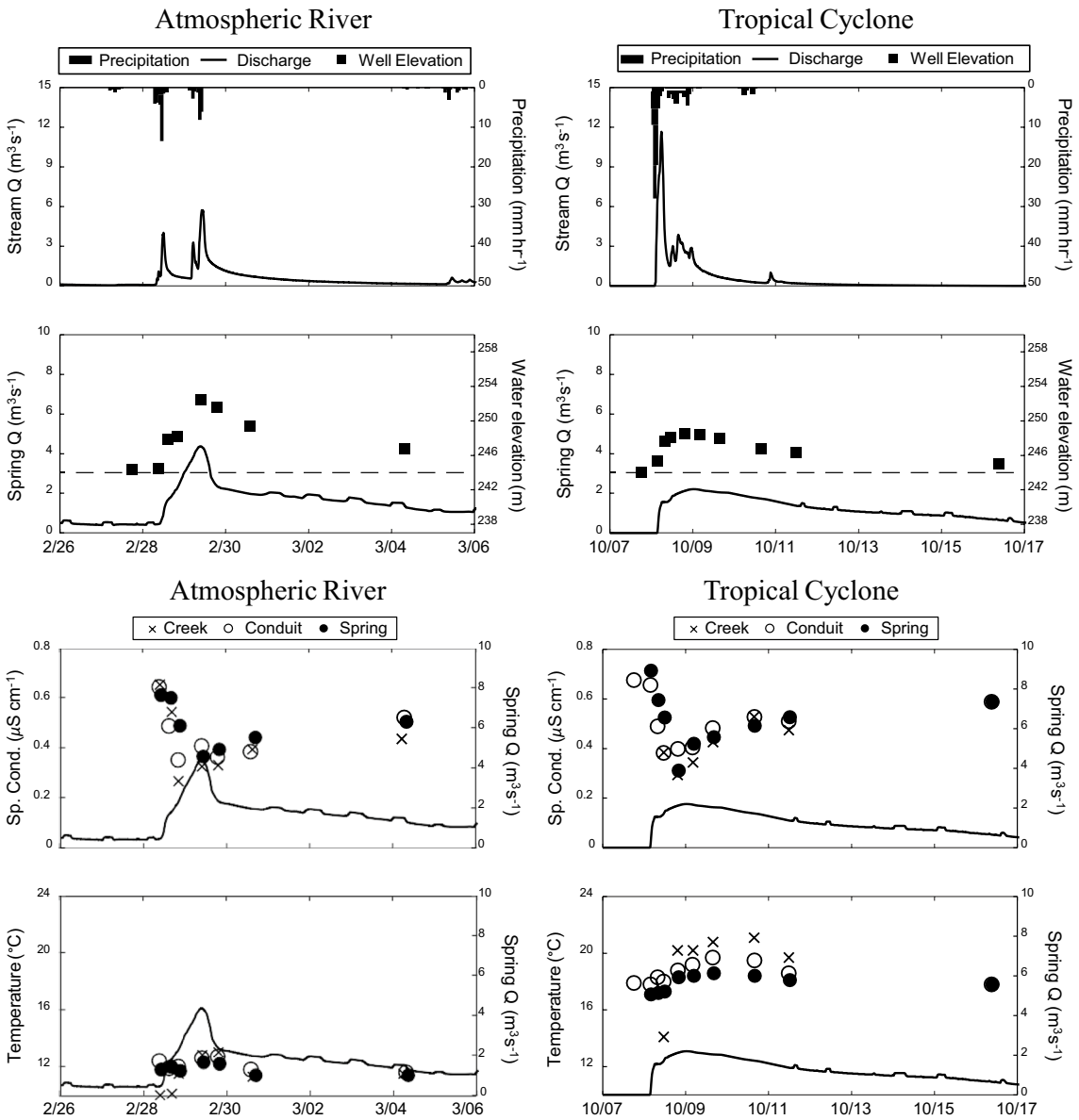

Fig. 5 Precipitation, stream flow, groundwater elevation (above mean sea level), spring discharge, specific conductance, and temperature data results. The dashed horizontal line on the second row represents the elevation of Royal Spring. The surface stream discharge peaks quickly to rainfall input relative to spring discharge. The groundwater elevation in the well intersecting the conduit corresponds closely to spring discharge. Specific conductance and temperature of the conduit and spring are largely influenced by the surface creek, and are either warmed or cooled depending on season

(i.e., over three-quarters in this study watershed; Husic et al. 2017a). Furthermore, the extent of this loss can vary based on pre-event hydrologic conditions, and thus, extreme events that occur during different seasons (e.g., atmospheric rivers and tropical cyclones) are expected to produce differing responses. Since contaminant transport is heavily influenced by hydrology (Padilla and Vesper 2018), we may expect to see rainfall intensity which also impacts on the loading and timing of NO_3^- delivery to the spring.

Water-quality and environmental tracer analyses

Specific conductance varied greatly over the course of the atmospheric river and tropical cyclone events and was impacted by the initial dilution via quick flow and a return to baseflow conditions at the end of recession (Fig. 5). During

the tropical cyclone, specific conductance varied slightly more than it did for the atmospheric river due to two factors (1) the highly conductive antecedent water, arising from an extended dry period, and (2) the overloading of the system with an annual maximum of poorly conductive rainfall. Temporally, changes in specific conductance were similar at all three locations over the course of both events. The temperature did not vary significantly during the atmospheric river event, even with the influx of stream water, as the air temperature during this time was similar to the background aquifer water temperature (~ 13 °C). On the other hand, the temperature shift between surface and subsurface pathways was more noticeable during the tropical cyclone, which occurred in early fall. The significantly warmer surface water, abstracted by swallets, markedly increased the temperature of conduit water. During longitudinal transport (from the Phreatic Conduit to Royal Spring), convective heat losses at the conduit walls cooled the water close to that of the background aquifer temperature. During both events, temperature maxima tended to lag peak discharge, indicating the arrival of warmer water stored in the epikarst and soil.

High specific conductance reflects the water–rock exchange of solutes and increases with longer water residence time (Winston and Criss 2004). For example, prior to the atmospheric river event, the specific conductance in the creek was also high, which was attributed to a several-week period without streamflow, thus, providing adequate time for the limestone bedrock to exchange ions with standing pools of water. In a study comparing conservative and non-conservative tracers in a karst conduit, Luhmann et al. (2012) found that the temperature lag is more apparent than the specific conductance lag, showing agreement with our results. This is associated with thermal losses to the surrounding rock which produces a temperature pulse less than that of the actual groundwater velocity (Molson et al. 2007).

The concentration of NO_3^- was consistently higher in the subsurface than it was in the surface creek for both events (Fig. 6). For the atmospheric river event, surface creek NO_3^- concentration was initially ~ 1 mg N L^{-1} and increased thereafter as runoff and lateral soil flow, more concentrated in NO_3^-, contributed to streamflow. However, at the conduit and spring sites, an initial decrease in NO_3^- concentration reflected the mixing of antecedent aquifer water with less-concentrated surface water. Thereafter, NO_3^- concentration at all three sites peaked a few days after maximum spring discharge and then slowly

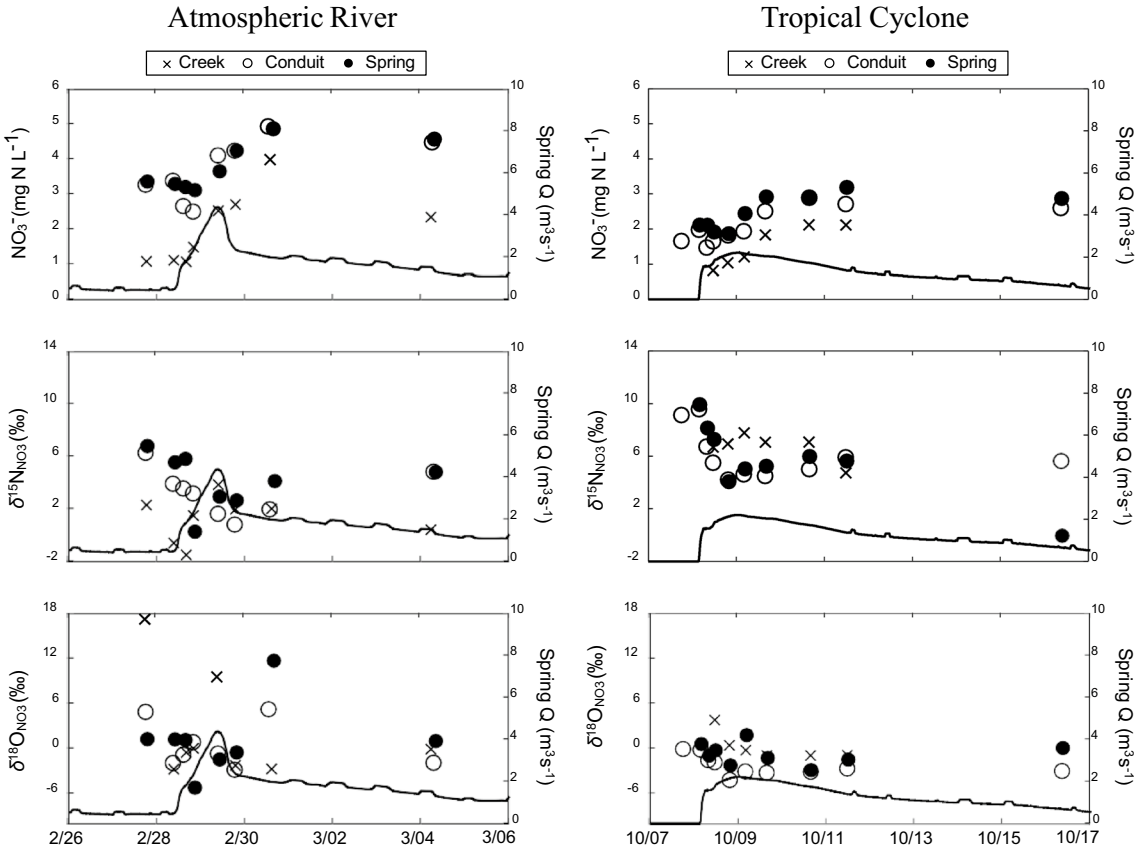

Fig. 6 NO_3^-, $\delta^{15}N_{NO3}$, and $\delta^{18}O_{NO3}$ signatures of creek, conduit, and spring water during two extreme events. NO_3^- is initially diluted by surface quick flow during both events as are $\delta^{15}N_{NO3}$ and $\delta^{18}O_{NO3}$. Thereafter, all three parameters tend to increase

return to baseflow levels over the subsequent weeks. The temporal evolution of $\delta^{15}N_{NO3}$ and $\delta^{18}O_{NO3}$, over the course of both events, was similar at the conduit and spring sites. At the onset of the event, $\delta^{15}N_{NO3}$ and $\delta^{18}O_{NO3}$ values at the spring and conduit decreased due to surface stream contributions. Thereafter, $\delta^{15}N_{NO3}$ and $\delta^{18}O_{NO3}$ tend to increase during hydrograph recession. However, we also observed a large degree of variability in the values $\delta^{15}N_{NO3}$ and $\delta^{18}O_{NO3}$ during both the rising and falling limbs of the hydrograph. This significant variability, over short time scales, has been observed in rivers and streams (e.g., Pellerin et al. 2009), and is likely associated with the lack of a single dominant physical or biological mechanism controlling isotopic composition, but rather the coexistence of several complex mechanisms, such as fractionation and mixing.

The difference in NO_3^- concentration between surface and subsurface flow paths may be associated with the leaching of NO_3^- from soil and epikarst pathways. Initially, the NO_3^- concentration is diluted by quick flow and, as the system transitions from quick-flow to slow-flow dominance, the concentration reaches a peak during the period of inferred maximum drainage from the epikarst and soil storages. Others have also noted that geochemical time responses in karst tend to be delayed relative to discharge response (e.g., Winston and Criss 2004). Whereas some researchers have indicated that the initial spikes in spring NO_3^- concentration can be associated with mobilization of NO_3^- accumulated within the watershed (e.g., Toran and White 2005; Huebsch et al. 2014), our data set suggests, otherwise, at least in the case of telogenetic fluviokarst systems. In karst watersheds with a pronounced quick-flow contribution (i.e., high connectivity between surface and subsurface pathways), an initial dilution (rather than mobilization) of NO_3^- is likely to occur as intense rainfall is first routed to large fissures and shafts rather than through soil pores. Thereafter, as connectivity is re-established via wetting of the epikarst, highly concentrated NO_3^- in the soil and vadose zone is introduced to active subsurface pathways thus increasing spring NO_3^- concentration. Others have noted that when soil moisture is low and soils are well aerated, nitrification can generate large pools of NO_3^-, which may potentially be flushed during storm events (Christopher et al. 2008; Buda and DeWalle 2009). The connectivity of the epikarst to the larger soil basin may have an analogous effect on NO_3^- delivery within the context of karst: NO_3^- stored within the soil may be higher due to production by nitrification and concentration by evaporation, whereas NO_3^- in the water-logged epikarst aquifer may have experienced a degree of denitrification. While the rising limb and peak hydrograph periods are associated with the highest NO_3^- concentrations in some surface streams (Inamdar et al. 2004; Rusjan et al. 2008), the results of this study indicate that the highest NO_3^- concentrations may appear days after the storm peak in mature karst systems.

Observed $\delta^{15}N_{NO3}$ values at the spring during both events fall within the range of NO_3^- derived from soil mineralization (0 to +9‰), ammonium (NH_4^+) in fertilizer and precipitation (−10 to +5‰), and manure and septic waste (0 to +25‰) (Kendall et al. 2007). The initial decrease in $\delta^{15}N_{NO3}$ and $\delta^{18}O_{NO3}$ at the spring during the rising limb of both events was likely associated with inflowing N from fertilizer, soil, and precipitation sources. The $\delta^{15}N_{NO3}$ and $\delta^{18}O_{NO3}$ values tend to reach stability (4 and 0‰, respectively) a few days after the peak of both events, indicating that the source of NO_3^- during spring recession is likely derived from soil mineralization. The observed NO_3^-, $\delta^{15}N_{NO3}$, and $\delta^{18}O_{NO3}$ responses at Royal Spring are indicative of influence from quick-, intermediate-, and slow-flow paths. The initial decreases in NO_3^- were likely due to dilute quick-flow recharge, whereas subsequent increases were associated with intermediate-flow drainage from epikarst storage. The observed NO_3^- peak was likely associated with soil-zone flushing, while the ultimate return to baseflow concentrations was brought upon by phreatic matrix recharge.

The δ^2H_{H2O} and $\delta^{18}O_{H2O}$ signatures of the three sampling sites were similar across the entirety of the atmospheric river event with a small peak during maximum spring discharge, suggesting only slight differences in the origin of water flushing during the event (Fig. 7). The variability observed in $\delta^{13}C_{DIC}$ also indicates a quick response of relatively depleted $\delta^{13}C_{DIC}$ during peak storm conditions and a return to isotopically heavier $\delta^{13}C_{DIC}$ during the baseflow recession. On the other hand, the δ^2H_{H2O}, $\delta^{18}O_{H2O}$, and $\delta^{13}C_{DIC}$ signatures of samples collected during the tropical cyclone showed a stronger flushing of water and DIC through the watershed (Fig. 7). The variability in δ^2H_{H2O} and $\delta^{18}O_{H2O}$ values of water moving through the system was much greater during the tropical cyclone (Fig. 8a). During the rising limb of the event, signatures at all three locations showed a distinct shift towards lighter isotopes of water during peak activity (Fig. 8b, c). Subsequent baseflow returned the δ^2H_{H2O} and $\delta^{18}O_{H2O}$ values back to their pre-storm conditions (Fig. 8c).

The observed changes in δ^2H_{H2O} and $\delta^{18}O_{H2O}$ values are consistent with our knowledge of meteorology and karst hydrogeology. The trend of δ^2H_{H2O} and $\delta^{18}O_{H2O}$ values towards lighter isotopes during extreme events is a well-documented process, termed the "amount effect", of the greater depletion of heavier water molecules during periods of high precipitation rates (Lawrence and Gedzelman 1996). Tropical cyclones are efficient precipitation systems that deliver rainfall with $\delta^{18}O_{H2O}$ similar to that of seawater vapor (−12.3‰) (Lawrence and Gedzelman 1996). Indeed, $\delta^{18}O_{H2O}$ values approached a minimum of −11.0‰ during peak tropical cyclone activity, a dramatic shift from the typical value of −5.0‰ (Fig. 8c). The highly depleted water

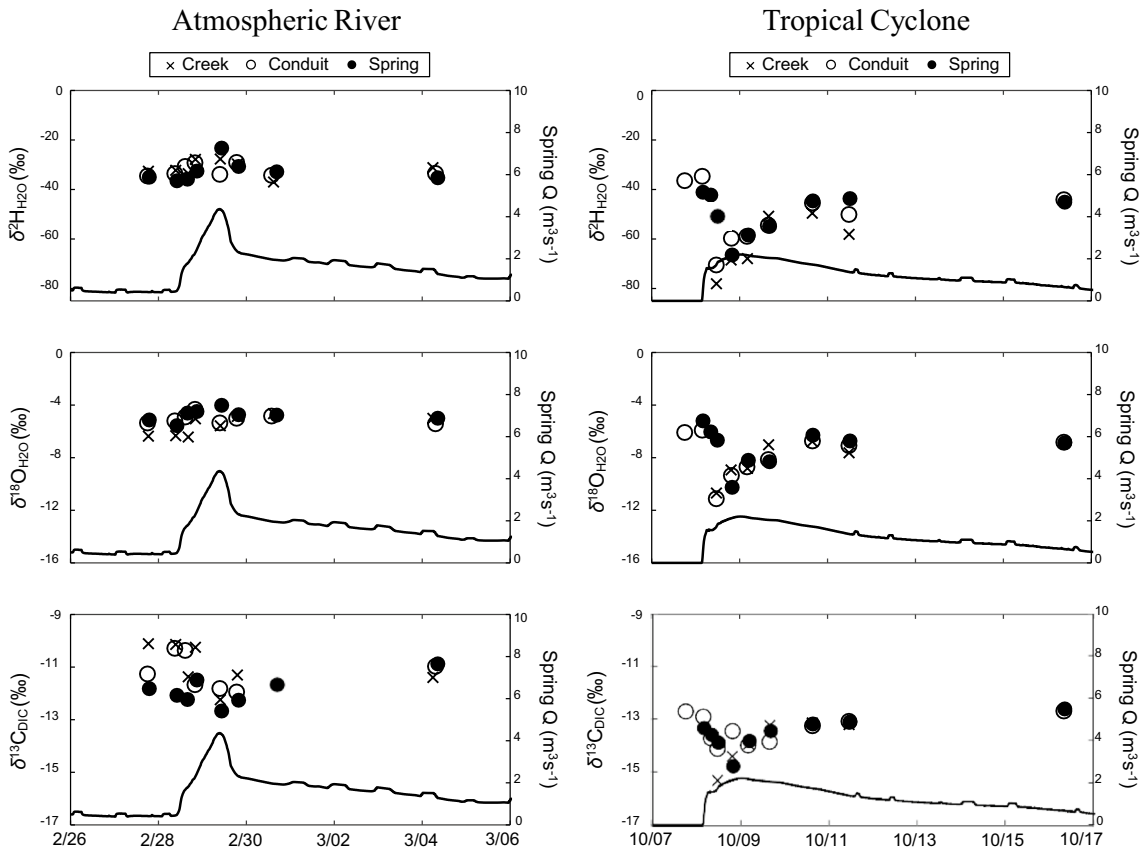

Fig. 7 δ^2H_{H2O}, $\delta^{18}O_{H2O}$, and $\delta^{13}C_{DIC}$ signatures of creek, conduit, and spring water during two extreme events. Variability is limited in δ^2H_{H2O} and $\delta^{18}O_{H2O}$ signatures during the atmospheric river event, but the tropical cyclone (i.e., Hurricane Nate) delivered highly depleted rain water (close to that of sea surface water vapor $\delta^{18}O_{H2O} \sim -12‰$). Likewise, $\delta^{13}C_{DIC}$ data also indicate the delivery of highly depleted DIC during the tropical cyclone

from Hurricane Nate (demoted to a tropical storm before reaching central Kentucky) indicates the ability of coastally derived inland storms to alter local hydrology. In addition, the observed changes in the $\delta^{13}C_{DIC}$ signature are consistent with the changing of source waters in a karst watershed (Lee and Krothe 2001). Although no DIC concentration data were collected during this study, the DIC isotope composition can be used as a qualitative indicator of changes to discharging water. $\delta^{13}C_{DIC}$ values of DIC generated by biological processes in the soil and epikarst zones tend to be lighter than those of the deeper groundwater caused by dissolution of an inorganic source of carbon (i.e., bedrock) to phreatic waters (Knierim et al. 2013). Thus, it can be inferred that the transition from lighter to heavier $\delta^{13}C_{DIC}$ over the hydrograph recession (Fig. 7) may be indicative of a return from intermediate (soil and epikarst) to slow (phreatic) flow drainage.

Our comprehensive water-quality and environmental tracer data set was vital to understanding the physical and biogeochemical processes that occurred during two structurally different extreme events. Though environmental isotope tracers have received widespread use in karst (e.g., Lee and Krothe 2001; Buda and DeWalle 2009; Albertin et al. 2012; Yue et al. 2018), we provide a data set with unique components including: high-frequency (up to hourly) isotope tracer collection during atmospheric river and tropical cyclone events, longitudinal water-quality and isotope tracer data from within a karst conduit, and surface and subsurface event data using a suite of isotopes ($\delta^{15}N_{NO3}$, $\delta^{18}O_{NO3}$, $\delta^{13}C_{DIC}$, $\delta^{2}H_{H2O}$, and $\delta^{18}O_{H2O}$). A limitation of this data set is the number of extreme events included. While our data set is composed of only two events, the collection of such data is difficult due to the unpredictability and the timing of intense hydrologic activity; the uncertainty associated with the amount of rainfall and whether enough will be generated to consider an event 'extreme'; and the incidence of certain extreme events that may have recurrence intervals of a year or longer. To the second point, we collected data for four total events, but, by the conclusion of the calendar year, two of the events collected earlier in the study fell out of the 95th percentile (i.e., the threshold definition for 'extreme' used in this study). Thus, the data set which we present is a great contribution as it includes half of the most extreme

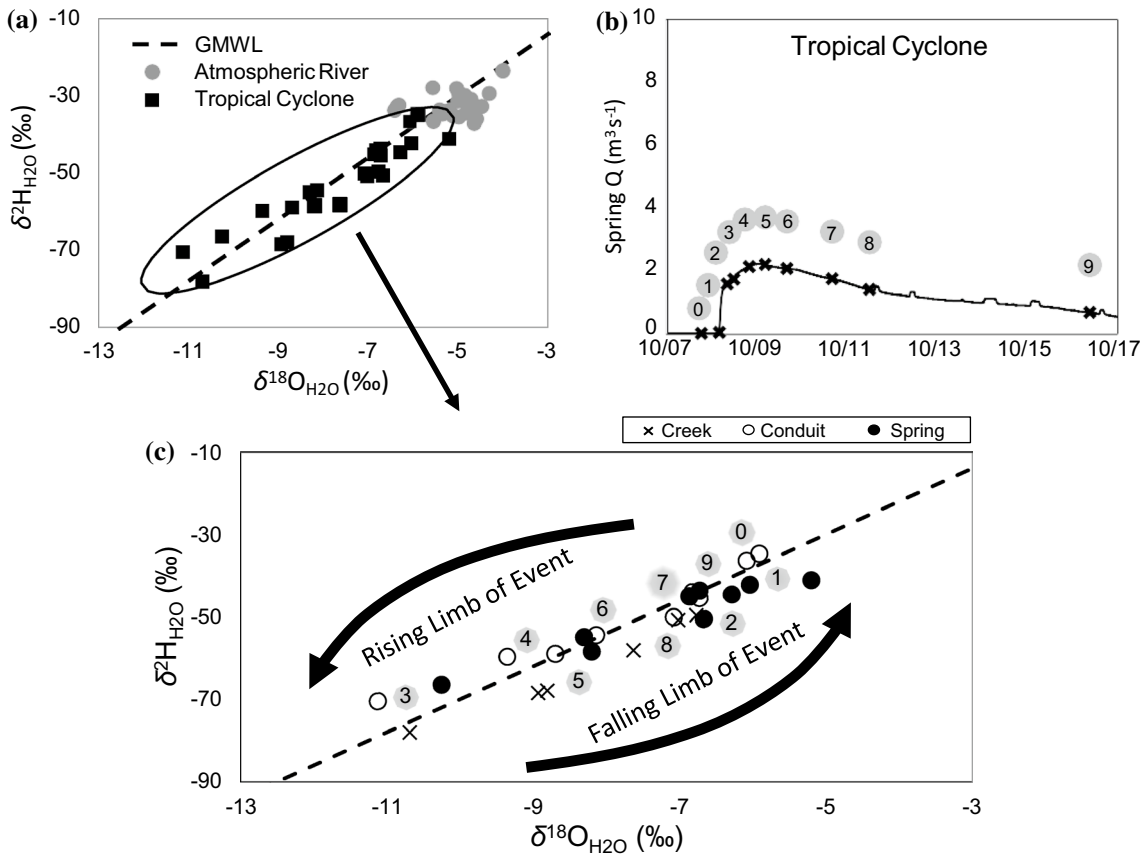

Fig. 8 **a** δ^2H_{H2O} and $\delta^{18}O_{H2O}$ of all samples collected for the two storm events. **b** Sample sets collected from creek, conduit, and spring in relation to the tropical cyclone spring hydrograph. **c** Zoom-in on the tropical cyclone event. δ^2H_{H2O} and $\delta^{18}O_{H2O}$ signatures show an appreciable effect of coastal water delivery to inland Kentucky via the shift towards lighter isotopes during peak event activity. Numbers inset in gray circles in **c** indicate the approximate δ^2H_{H2O} and $\delta^{18}O_{H2O}$ average of creek, conduit, and spring samples corresponding to the sets identified in **b**. *GMWL* global mean water line

events of 2017, where both events had structurally unique meteorological origins and occurred during significantly different parts of the year.

Hydrograph and loadograph separation analyses

Recession analysis indicates the presence of two inflection points, on the falling limb of the spring hydrograph, which divide the contributions of quick-, intermediate-, and slow-flow pathways (Fig. 9). The atmospheric river event was characterized by a steeper initial quick-flow recession and then gradual decreases in slope for the intermediate- and slow-flow components (Fig. 9a). The quick–intermediate inflection point occurred 0.5 days after the peak of the event and the intermediate–slow inflection point occurred 5.8 days after the peak discharge. The sudden decrease in discharge that occurred on 3/16/2017 was not believed to be a natural occurrence, but rather an artifact of water treatment plant operations. We have confidence that the drainage prior to and after this sudden change in discharge arises from the same reservoir as the slope is relatively unchanged. The tropical cyclone event had a more gradual quick-flow recession component, followed by a milder intermediate-flow component, and a slightly steeper slow-flow component (Fig. 9b). The quick–intermediate and intermediate–slow inflection points occurred 2.5 and 6.3 days, respectively, after peak event discharge.

The atmospheric river event hydrograph is characterized by a more typical shape with a steep initial recession followed by gradually milder recessions. The fall tropical cyclone event had a less typical hydrograph recession resulting from the large volume of rainfall, on dry soils, and infiltration that occurred in a relatively short period of time. This type of behavior has been observed during extreme events in other karst studies, where hydrographs may potentially diverge from their typical behavior, with recessions that may alternate in convexity (Herman et al. 2008). This deviation from typical hydrograph behavior is associated with non-linearity induced by drainage from the other reservoirs (Herman et al. 2008). In our study, the mild

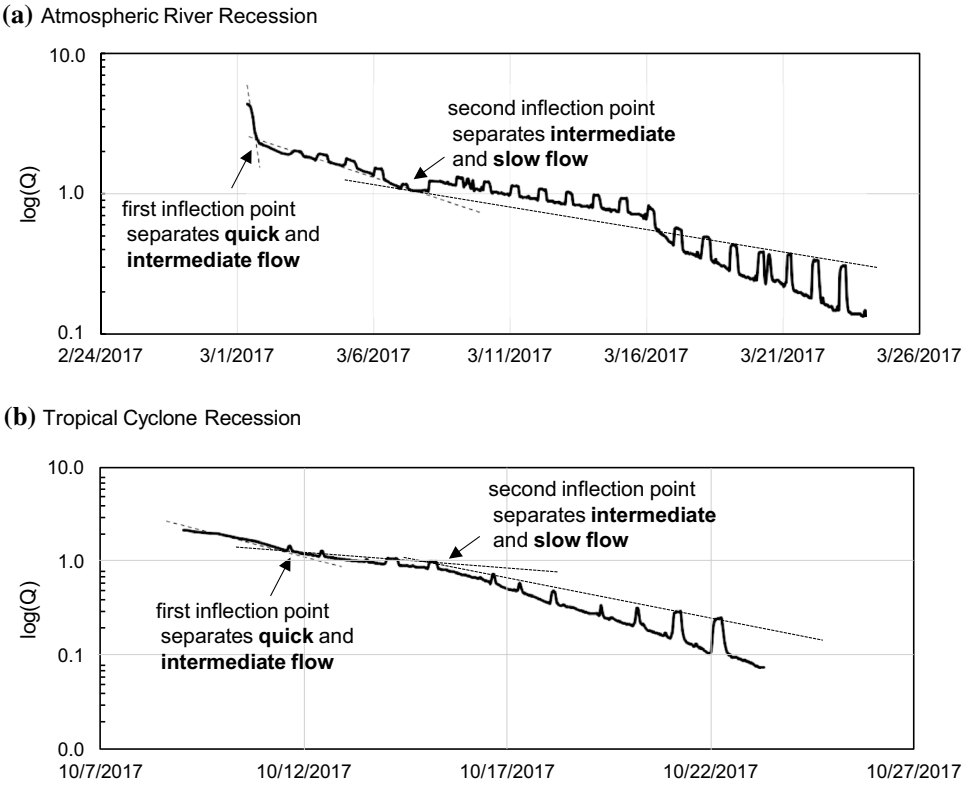

Fig. 9 Method for hydrograph and loadograph separation analysis. **a** During the atmospheric river event, quick–intermediate- and intermediate–slow-flow inflection points occur 0.5 and 5.8 days, respectively, after hydrograph peak. **b** During the tropical cyclone, quick–intermediate- and intermediate–slow-flow inflection points occur 2.5 and 6.3 days, respectively, after hydrograph peak. Abrupt spikes and drops in the recession hydrographs are the result of periodic pumping, by a water treatment plant, directly upstream of the v-notch weir where water depth is gaged. These abstractions were considered when estimating the recession lines

slope of the hydrograph recession (starting on 10/12/2017 in Fig. 9b) likely corresponds to a perched-reservoir condition influenced by the recently wetted epikarst and soil. The perched aquifer may provide a storage volume of water that is highly influenced by the soil but lacks hydrologic connectivity to the primary springhead during hydrologically inactive periods. As the epikarst and soil are reconnected to the aquifer, they provide the opportunity to deliver water highly concentrated in NO_3^-.

The loadograph results have a similar shape to the hydrograph results (Fig. 10). The loadograph quick flow ceases at the first inflection point of the recession and intermediate recharge ends at the second inflection point (identified by dashed lines). Loadograph analysis shows that quick-flow pathways during the tropical cyclone contribute longer to NO_3^- loading (Fig. 10b) than during the atmospheric river (Fig. 10a). The average NO_3^- loading from the catchment during the atmospheric river and tropical cyclone events was 3.6 and 1.5 g N ha^{-1} h^{-1}, respectively. For the atmospheric river event, the quick-flow pathway contributed 10.1%, the intermediate pathway contributed 36.9%, and the slow-flow pathway contributed 53.0% of total event NO_3^- (Fig. 10c). Results for the fall event were more heavily impacted by the high-intensity rainfall with 20.7%, 28.7%, and 50.6% of total event NO_3^- attributed to quick-flow, intermediate-, and slow-flow pathways, respectively (Fig. 10c). The high loads that occur from pathways draining epikarst and phreatic waters are a combination of high pathway discharge and NO_3^- concentration. The intermediate pathway delivered the highest NO_3^- concentration for both events, while the quick-flow pathway diluted the NO_3^- concentration.

Nitrogen loading from our watershed over the course of two extreme events (1.5–3.6 g N ha^{-1} h^{-1}) is slightly less than other well-drained agriculturally impacted watersheds both with karst features (3.13 to 7.60 g N ha^{-1} h^{-1}) and without karst features (2.64–2.81 g N ha^{-1} h^{-1}) (Mellander et al. 2012; Fenton et al. 2017). Fenton and others separated flow into four components (conduits, and large, medium, and small fissures), and they note that the proportion of NO_3^- loading increases with storm intensity, showing agreement with our results. However, they suggest that the highest flow-weighted means are in the quick-flow transfer pathways, whereas our results indicate dilution by quick flow and concentration by intermediate pathways (Fig. 10c). This discrepancy may potentially be due to the difference in watershed characteristics, whereby the Fenton et al.'s (2017) study, a dairy farm in Ireland, is primarily recharged by diffuse flow, whereas the Cane Run watershed has considerable recharge from dilute surface water. This result highlights that aquifer pathway connectivity to the surface can influence NO_3^- concentrations at the spring.

Integration of the hydrograph and loadograph for each event revealed surprising similarities. First, the maximum percentage of total storm water conveyed by the quick-flow

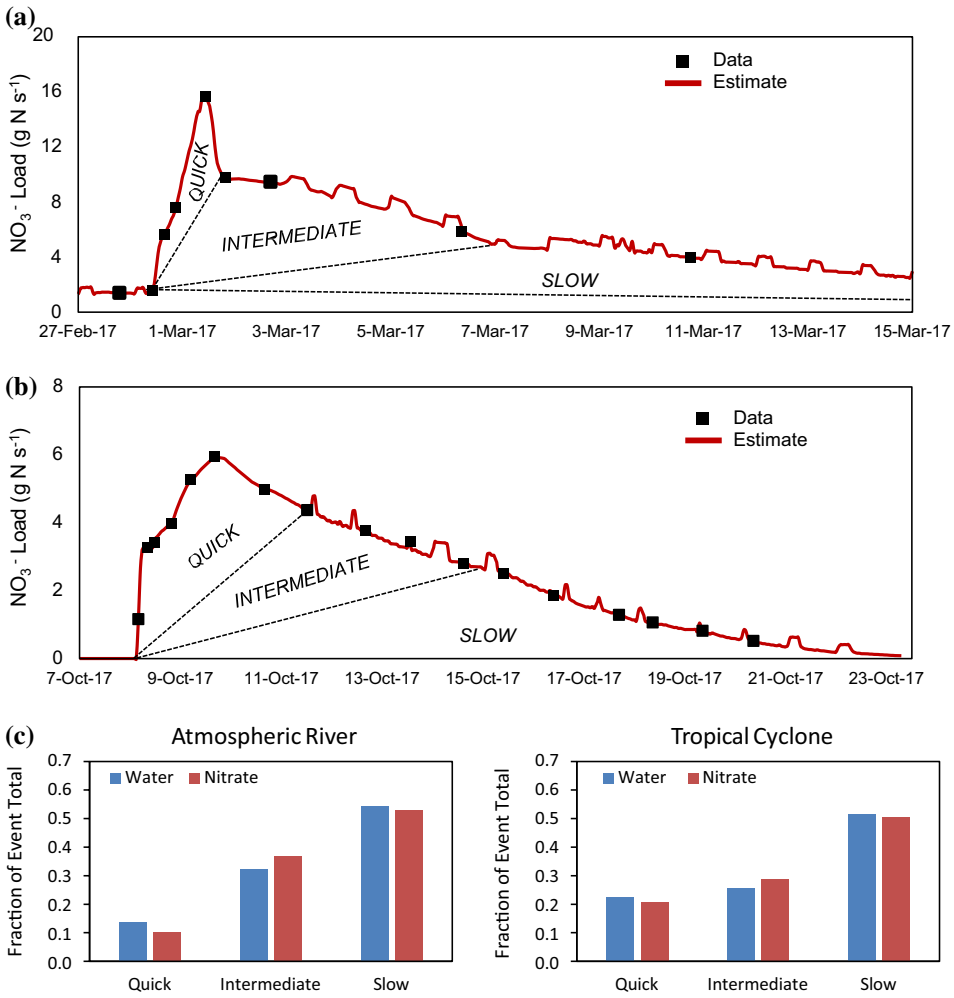

Fig. 10 **a** Atmospheric river loadograph results separated into three separate pathways (quick, intermediate, and slow flow). The dashed lines direct to the recession inflection points identified in the Fig. 9 analysis. **b** Same as **a** but for the tropical cyclone event. **c** The fraction of total event discharge and NO^- loading per pathway for the atmospheric river and tropical cyclone events

pathway for the two events was only 21% (Fig. 10c). This result was unexpected as the Cane Run watershed is highly karstified, pirates all streamflow from the surface creek for over 80% of the year, and has a hydrologic response time on the same order of magnitude as the surface stream, indicating a large quick-flow influence (Husic et al. 2017a, b). We anticipated that the contribution by quick-flow would be considerably greater as the monitored events were two of the four largest of the year. Rather, it was the intermediate- and slow-flow pathways that dominated loading with water derived from the epikarst and phreatic bedrock matrix accounting for approximately 30% and 50% of the total water and N load, respectively. A second similarity was the pathway NO_3^- behavior for both events. Irrespective of the differences in NO_3^- concentration from the atmospheric river to the tropical cyclone, which ranged from a maximum of 3–5 mg N L^{-1} (Fig. 6), both events were characterized by the initial dilution via quick flow and subsequent concentration via the intermediate-flow draining the epikarst (Fig. 10c). While the results of this study are likely system-dependent, and may vary for different karst systems, this result suggests that, when adequate hydrologic connectivity is established across the various karst pathways (such as in the case of extreme events), the net contribution of pathways may act predictably regardless of the level or extent of aquifer contamination.

Nutrient lag effect in karst aquifers

The nutrient lag effect during extreme events in karst aquifers was assessed through hydrograph and loadograph separation analyses. In addition, the authors attempted to investigate the lag effect by utilizing a suite of collected environmental tracer data and end-member mixing analysis, but were unsuccessful for a couple of important reasons: (1) the high spatiotemporal heterogeneity of the epikarst and (2) the non-stationarity of source end-members during extreme event activity. To the first point, the epikarst in our study area varies in terms of its spatial extent and thickness—from parts that are exposed to the surface to others that are buried beneath thick soil layers (Phillips et al. 2004). This spatial heterogeneity complicates the collection of a 'representative'

epikarst sample from within the watershed. To the second point, the extreme events monitored in this study had profound impacts on hydrologic processes in the watershed as system dynamics became overwhelmed by extreme rainfall totals. This overwhelming of system dynamics caused end-members to lose their stationary signal, thus, violating a core assumption of conservative unmixing analysis. However, we were able to use our hydrograph unmixing together with the time series of environmental data to qualitatively provide some insight into how the end-members contribute water and nutrients to the spring.

We used the recession analysis to successfully separate the hydrograph into its three flow pathways (quick, intermediate, and slow flow) and plotted the pathways against water-quality and isotopic measurements (Fig. 11) to investigate temporal changes in data with regard to pathway contribution. For the atmospheric river event, specific conductance, $\delta^{13}C_{DIC}$, $\delta^{2}H_{H2O}$, and $\delta^{18}O_{H2O}$ have maxima or minima that occur during the influence of quick-flow and before peak intermediate flow. Upon passing of the quick-flow component, the observed values for each measurement return to pre-storm conditions. NO_3^-, temperature, $\delta^{15}N_{NO3,}$ and $\delta^{18}O_{NO3}$ experience a 'lag effect' relative to other measurements. The values of NO_3^-, $\delta^{15}N_{NO3,}$ and $\delta^{18}O_{NO3}$ continue to increase after quick flow ceases, and even after peak intermediate flow, indicating that intermediate flows can potentially be subdivided into epikarst and soil pathways. The NO_3^- concentration maxima occurred approximately 1.3

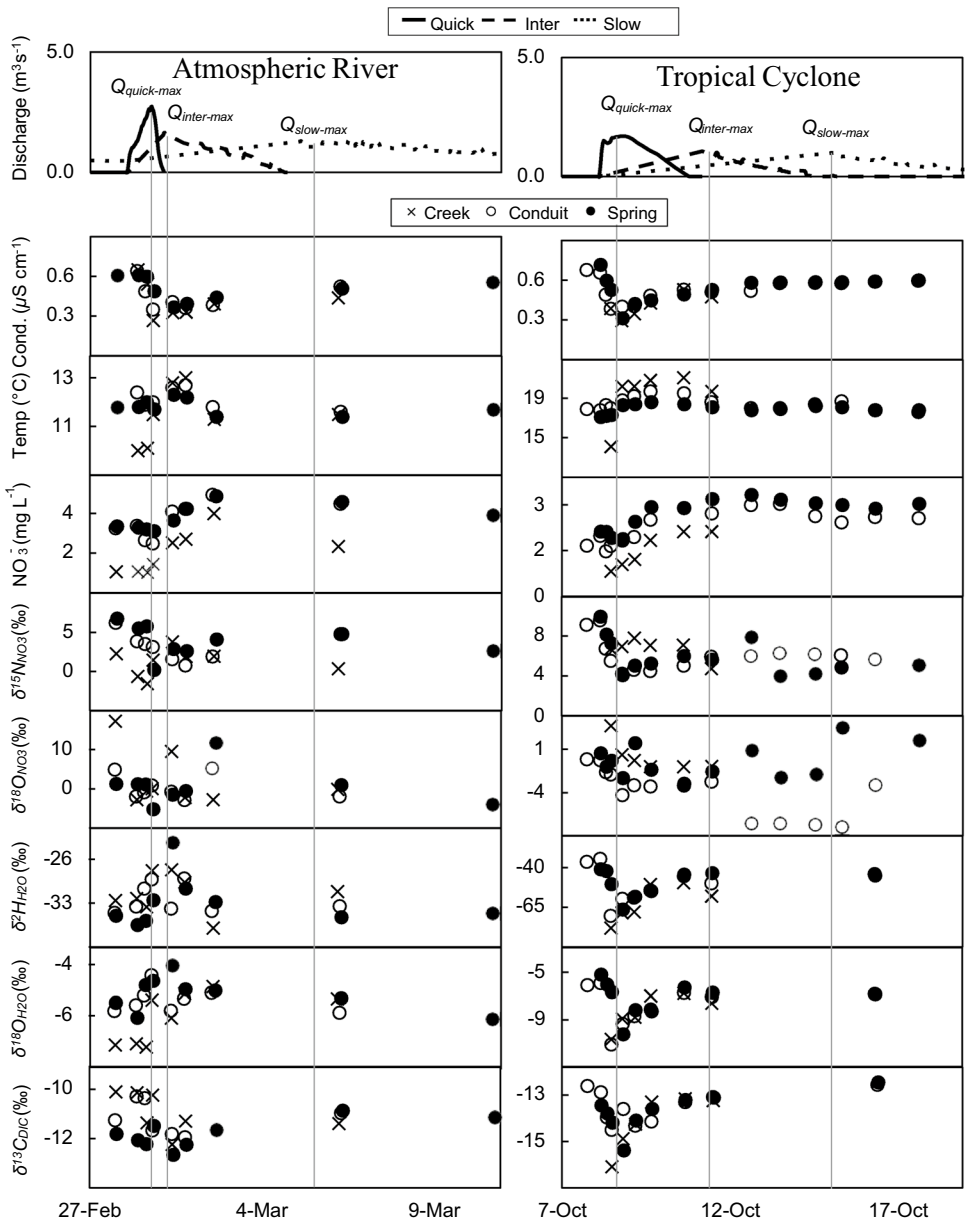

Fig. 11 Temporal changes in water-quality and environmental isotopes. The top two subplots show discharge for the three pathways (quick, intermediate, and slow) with maximums identified. Lines from each max discharge to subplots below are drawn to highlight temporal lags

days after the flow hydrograph peak and 0.8 days after the transition from quick flow to intermediate flow. The tropical cyclone event experiences similar behavior, whereby specific conductance, $\delta^{13}C_{DIC}$, $\delta^{2}H_{H2O}$, and $\delta^{18}O_{H2O}$ tend to peak around maximum quick-flow discharge (Fig. 11). On the other hand, NO_3^- continues to increase days after peak intermediate flow. The NO_3^- concentration maxima occurred 3.6 days after the peak of the event and 1.1 days after the quick-flow–intermediate inflection point. $\delta^{15}N_{NO3}$ and $\delta^{18}O_{NO3}$ at the spring have minima located after the NO_3^- maxima.

In the case of both extremes, hydrograph pathway separation alone cannot predict peak NO_3^- concentration in spring water. The points of inflection on the hydrograph which separate sources do not coincide with the NO_3^- concentration maxima. The shift from dilute source to concentrated source occurs a few days prior (t_{lag}) to the maximum NO_3^- concentration (Fig. 12). Rather, the intermediate flow is conceptualized to experience a shift in porosity, likely associated with a source-water change from epikarst fissures to soil micropores. The delayed arrival of nitrate-laden water from the soil into the epikarst results in a nutrient lag effect, whereby maximum discharge from the intermediate pathway (associated with maximum epikarst contribution) does not equal the peak concentration in that pathway (Fig. 12). This result suggests that the epikarst does not have its own constant concentration but rather a relatively dilute component (fissures) and a relatively concentrated component (soil). As transport of N through a watershed is primarily controlled by hydrology (Bauwe et al. 2015; Sinha and Michalak 2016), the accurate discretization of sources is paramount to undertaking effective mitigation efforts. Our results indicate that a more discretized conceptual model of pathways may be needed to predict peak N concentration in rivers, particularly in karst terrains.

While consideration for the soil-derived peak in NO_3^- concentration is a further improvement in our understanding of N pathways, the existing literature of soil processes helps to provide support for this concept. Accumulation and leaching of NO_3^- from the soil are recognized as a driving factor in the rising concentrations of NO_3^- in surface and subsurface waters draining agricultural systems (Di and Cameron 2002). While discharge may initially dilute the NO_3^- signal (Miller et al. 2017), it also provides the mechanism to activate pathways and transport concentrated NO_3^- down-gradient (Baran et al. 2008). Studies in tile-drained agricultural systems, which have been likened to karst (Schilling and Helmers 2008), have noted that the initial flow may bypass highly concentrated soil zones and, only after significant wetting, is connectivity established between the highly concentrated zones and preferential flow paths (Klaus et al. 2013; Ford et al. 2018). Thus, soil

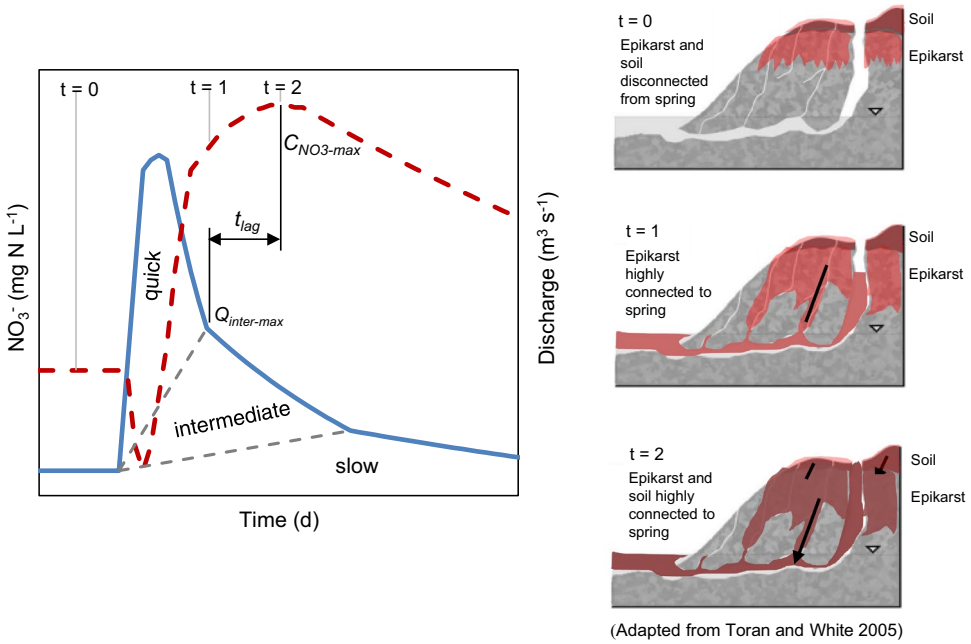

Fig. 12 Conceptualized response of NO_3^- (dashed red line) and discharge (solid blue line) to extreme events in a mature karst watershed. Prior to a storm event, when the epikarst and soil are disconnected from the spring, NO_3 concentrations are constant ($t=0$). An initial decrease of NO_3 concentration (C_{NO3}) is caused by dilute storm recharge. Nitrate concentration increases as intermediate (epikarst + soil) flow (Q_{inter}) becomes more dominant ($t=1$). There is a time lag between peak intermediate discharge and peak NO_3 concentration (t_{lag}). This lag occurs as pre-storm epikarst water drains and is recharged by nitrate-rich soil water ($t=2$). Finally, as the hydrograph recedes, NO_3 concentrations return to baseflow levels

water NO_3^- becomes rapidly transported during and after intense storm conditions (Huebsch et al. 2014). The time lag between peak intermediate flow and concentration of other geochemical pollutants such as pesticides in a chalk aquifer agrees with our results, and is associated with a retarding effect of less mobile water within smaller pores (Baran et al. 2008). In the study by Baran et al. (2008), a NO_3^- peak was observed following large events, which would indicate mobilization by quick flow; however, the sampling frequency used in that study was approximately 10 days (over the course of 17 years), which may overlook the initial quick-flow dilution and subsequent intermediate-flow concentration that can potentially happen within hours to days, respectively, of incident rainfall. Long-term studies are useful for assessing changing land practices and climate drivers (Xue et al. 2009), but we recommend high-frequency sampling during storm events to aid in de-coupling pathways. Given that a shift from fissure-scale porosity in the epikarst to pore-scale porosity in the soil can impact peak NO_3^- concentration in spring water, further investigation of this shift is crucial to meeting water-quality needs.

Conclusions

The conclusions of the paper are as follows:

1. Inland impacts of an atmospheric river and tropical cyclone produced the number one and four ranked rainfall events in 2017 for the basin. Hydrologic pathway responses from the two extremes were different due to rainfall characteristics of the storms. The atmospheric river delivered low-intensity rainfall on wet soils, while the tropical cyclone brought high-intensity rainfall on dry soils.
2. Water-quality and environmental tracer data showed similar responses regardless of event structure (atmospheric river or tropical cyclone). In general, all stable isotope measurements, including $\delta^{15}N_{NO3}$, $\delta^{18}O_{NO3}$, $\delta^{2}H_{H2O}$, $\delta^{18}O_{H2O}$, and $\delta^{13}C_{DIC,}$ showed decreases in per mil values during quick-flow dominance relative to times when pathways draining the epikarst and phreatic bedrock matrix dominated. Local minima or maxima of water and DIC isotope compositions, as well as specific conductance, coincided with hydrograph peaks for both events. Local maxima of NO_3^- concentration lagged behind hydrograph peaks for both events as did maxima and minima of $\delta^{15}N_{NO3}$ and $\delta^{18}O_{NO3}$, although the isotopic data show variability that arose from the complex coupling of physical and biogeochemical processes.
3. The two extreme events showed similarities in mobilizing quick-, intermediate-, and slow-flow pathways of water and NO_3^- in the karst basin. Hydrograph and loadograph separation results show that quick-flow pathways account for less than 20% of transported water and NO_3^- during two of the year's most extreme events. The remaining water and NO_3^- loads are divided between the intermediate- (~30%) and slow-flow (~50%) pathways.
4. In the case of both extremes, hydrograph and loadograph pathway separation cannot predict the timing of NO_3^- concentration maxima. Rather, the intermediate flow is conceptualized to experience a shift in porosity from epikarst macropores and fissures to soil micropores. Furthermore, this change in source water and high degree of heterogeneity within a single pathway were obstacles to using a conservative end-member mixing analysis as the sources of nutrients during extreme events in karst are dynamic and non-stationary. Our results point out that a more discretized conceptual model of pathways may be needed to predict peak nutrient concentration in rivers, particularly those drain karst landscapes.
5. Differences in the results of this study with the other studies are attributed to variations in karst system characteristics, such as the degree of karstification, genetic carbonate structure (eogenetic vs telogenetic), spatial heterogeneity, surface–subsurface connectivity, and the extent of anthropogenic forcing on the landscape. Given these differences, it is vital to conduct experiments and monitoring operations that shed light on system-dependent processes, which, in turn, contribute to a greater understanding of karst function and help to bridge the gap across systems.

Acknowledgements The authors would like to thank the thematic issue guest editor Zexuan Xu and two anonymous reviewers for their insightful comments, which helped to greatly improve the quality of the manuscript. The authors would like to acknowledge the researchers and staff at the Kentucky Geological Survey, in particular, Chuck Taylor and James Currens, and the University of Arkansas Stable Isotope Laboratory. We also thank the Department of Civil Engineering at the University of Kentucky for partial funding of students involved with this research study. Finally, we gratefully acknowledge the financial support of this research under National Science Foundation Award 1632888. Data will be stored and publicly available at the following link: https://figshare.com/articles/EES_TI_Karst_Extremes/7170347.

References

Al Aamery N, Fox JF, Snyder M (2016) Evaluation of climate modeling factors impacting the variance of streamflow. J Hydrol 542:125–142. https://doi.org/10.1016/j.jhydrol.2016.08.054

Al Aamery N, Fox JF, Snyder M, Chandramouli CV (2018) Variance analysis of forecasted streamflow maxima in a wet temperate climate. J Hydrol 560:364–381. https://doi.org/10.1016/j.jhydrol.2018.03.038

Albertin AR, Sickman JO, Pinowska A, Stevenson RJ (2012) Identification of nitrogen sources and transformations within karst springs

using isotope tracers of nitrogen. Biogeochemistry 108:219–232. https://doi.org/10.1007/s10533-011-9592-0

Baran N, Lepiller M, Mouvet C (2008) Agricultural diffuse pollution in a chalk aquifer (Trois Fontaines, France): influence of pesticide properties and hydrodynamic constraints. J Hydrol 358:56–69. https://doi.org/10.1016/j.jhydrol.2008.05.031

Bauwe A, Tiemeyer B, Kahle P, Lennartz B (2015) Classifying hydrological events to quantify their impact on nitrate leaching across three spatial scales. J Hydrol 531:589–601. https://doi.org/10.1016/j.jhydrol.2015.10.069

Buda AR, DeWalle DR (2009) Dynamics of stream nitrate sources and flow pathways during stormflows on urban, forest and agricultural watersheds in central Pennsylvania, USA. Hydrol Process 23:3292–3305. https://doi.org/10.1002/hyp.7423

Burns DA, Miller MP, Pellerin BA, Capel PD (2016) Patterns of diel variation in nitrate concentrations in the Potomac River. Freshw Sci 35:1117–1132. https://doi.org/10.1086/688777

Cánovas CR, Hubbard CG, Olías M, Nieto JM, Black S, Coleman ML (2008) Hydrochemical variations and contaminant load in the Río Tinto (Spain) during flood events. J Hydrol 350:25–40. https://doi.org/10.1016/j.jhydrol.2007.11.022

Casciotti KL, Sigman DM, Hastings MG, Böhlke JK, Hilkert A (2002) Measurement of the oxygen isotopic composition of nitrate in seawater and freshwater using the denitrifier method. Anal Chem 74:4905–4912. https://doi.org/10.1021/ac020113w

Christopher SF, Mitchell MJ, McHale MR, Boyer EW, Douglas BA, Kendall C (2008) Factors controlling nitrogen release from two forested catchments with contrasting hydrochemical responses. Hydrol Process 22:46–62. https://doi.org/10.1002/hyp.6632

Cressman ER, Peterson WL (1986) Ordovician system. In: McDowell RC (ed) The geology of Kentucky: a text to accompany the geologic map of Kentucky. U.S. Geological Survey Professional Paper 1151-H, US

Debbage N, Miller P, Poore S, Morano K, Mote T, Marshall Shepherd J (2017) A climatology of atmospheric river interactions with the southeastern United States coastline. Int J Climatol 37:4077–4091. https://doi.org/10.1002/joc.5000

Di HJ, Cameron KC (2002) Nitrate leaching in temperate agroecosystems: sources, factors and mitigating strategies. Nutr Cycl Agroecosystems 64:237–256. https://doi.org/10.1023/A:1021471531188

Dodds WK, Smith VH (2016) Nitrogen, phosphorus, and eutrophication in streams. Inland Waters 6:155–164. https://doi.org/10.5268/IW-6.2.909

Drahovzal JA, Harris DC, Wickstrom LH, Walker D, Baranoski MT, Keith B, Furer LC (1992) The east continent rift basin: a new discovery. Kentucky Geological Survey 18 Ser. XI, Lexington

Fenton O, Mellander PE, Daly K, Wall DP, Jahangir MMR, Jordan P, Hennessey D, Huebsch M, Blum P, Vero S, Richards KG (2017) Integrated assessment of agricultural nutrient pressures and legacies in karst landscapes. Agric Ecosyst Environ 239:246–256. https://doi.org/10.1016/j.agee.2017.01.014

Fiorillo F (2014) The Recession of spring hydrographs, focused on karst aquifers. Water Resour Manag 28:1781–1805. https://doi.org/10.1007/s11269-014-0597-z

Florea LJ, Vacher HL (2006) Springflow hydrographs: eogenetic vs. telogenetic karst. Ground Water 44:352–361. https://doi.org/10.1111/j.1745-6584.2005.00158.x

Ford WI, Williams MR, Young MB, King KW, Fischer E (2018) Assessing intra-event phosphorus dynamics in drainage water using phosphate stable oxygen isotopes. Trans Am Soc Agric Biol Eng 61:1379–1392. https://doi.org/10.13031/trans.12804

Gao Y, Fu JS, Drake JB, Liu Y, Lamarque JF (2012) Projected changes of extreme weather events in the eastern United States based on a high resolution climate modeling system. Environ Res Lett https://doi.org/10.1088/1748-9326/7/4/044025

Gehre M, Geilmann H, Richter J, Werner RA, Brand WA (2004) Continuous flow 2H/1H and 18O/16O analysis of water samples with dual inlet precision. Rapid Commun Mass Spectrom 18:2650–2660. https://doi.org/10.1002/rcm.1672

Geyer T, Birk S, Licha T, Liedl R, Sauter M (2007) Multitracer test approach to characterize reactive transport in karst aquifers. Ground Water 45:36–45. https://doi.org/10.1111/j.1745-6584.2006.00261.x

Geyer T, Birk S, Liedl R, Sauter M (2008) Quantification of temporal distribution of recharge in karst systems from spring hydrographs. J Hydrol 348:452–463. https://doi.org/10.1016/j.jhydrol.2007.10.015

Hartmann A, Mudarra M, Andreo B, Marin A, Wagener T, Lange J (2014) Modelling spatiotemporal impacts of hydroclimatic extremes on groundwater recharge at a Mediterranean karst aquifer. Water Resour Res 50:6507–6521. https://doi.org/10.1002/2014WR015685.Received

Herman EK, Toran L, White WB (2008) Threshold events in spring discharge: evidence from sediment and continuous water level measurement. J Hydrol 351:98–106. https://doi.org/10.1016/j.jhydrol.2007.12.001

Huebsch M, Fenton O, Horan B, Hennessy D, Richards KG, Jordan P, Goldscheider N, Butscher C, Blum P (2014) Mobilisation or dilution? Nitrate response of karst springs to high rainfall events. Hydrol Earth Syst Sci 18:4423–4435. https://doi.org/10.5194/hess-18-4423-2014

Husic A (2015) Sediment organic carbon fate and transport in a fluviokarst. Master's Thesis. University of Kentucky. Lexington, Kentucky

Husic A (2018) Numerical modeling and isotope tracers to investigate karst biogeochemistry and transport processes. PhD Dissertation. University of Kentucky. Lexington, Kentucky

Husic A, Fox JF, Agouridis C, Currens JC, Ford WI, Taylor CJ (2017a) Sediment carbon fate in phreatic karst (Part 1): conceptual model development. J Hydrol 549:179–193. https://doi.org/10.1016/j.jhydrol.2017.03.052

Husic A, Fox JF, Ford WI, Agouridis C, Currens JC, Taylor CJ (2017b) Sediment carbon fate in phreatic karst (Part 2): numerical model development and application. J Hydrol 549:208–219. https://doi.org/10.1016/J.JHYDROL.2017.03.059

Inamdar SP, Christopher SF, Mitchell MJ (2004) Export mechanisms for dissolved organic carbon and nitrate during summer storm events in a glaciated forested catchment in New York, USA. Hydrol Process 18:2651–2661. https://doi.org/10.1002/hyp.5572

Jarsjö J, Chalov SR, Pietroń J, Alekseenko AV, Thorslund J (2017) Patterns of soil contamination, erosion and river loading of metals in a gold mining region of northern Mongolia. Reg Environ Chang 17:1991–2005. https://doi.org/10.1007/s10113-017-1169-6

Jarvie HP, Sharpley AN, Brahana V, Simmons T, Price A, Neal C, Lawlor AJ, Sleep D, Thacker S, Haggard BE (2014) Phosphorus retention and remobilization along hydrological pathways in karst terrain. Environ Sci Technol 48:4860–4868. https://doi.org/10.1021/es405585b

Katz BG, Griffin DW, McMahon PB, Harden HS, Wade E, Hicks RW, Chanton JP (2010) Fate of effluent-borne contaminants beneath septic tank drainfields overlying a karst aquifer. J Environ Qual 39:1181. https://doi.org/10.2134/jeq2009.0244

Kendall C, Elliott EM, Wankel SD (2007) Tracing anthropogenic inputs of nitrogen to ecosystems. In: Michener RH, Lajtha K (eds) Stable isotopes in ecology and environmental science 2nd edn. Blackwell Publishing, Hoboken, USA, pp 375–449

Klaus J, Zehe E, Elsner M, Külls C, McDonnell JJ (2013) Macropore flow of old water revisited: experimental insights from a tile-drained hillslope. Hydrol Earth Syst Sci 17:103–118. https://doi.org/10.5194/hess-17-103-2013

Knierim KJ, Pollock E, Hays PD (2013) Using isotopes of dissolved inorganic carbon species and water to separate sources of recharge in a Cave Spring, Northwestern Arkansas, USA. Acta Carsologica 42:261–276

Knight DB, Davis RE (2009) Contribution of tropical cyclones to extreme rainfall events in the southeastern United States. J Geophys Res Atmos 114:1–17. https://doi.org/10.1029/2009JD012511

Koenig LE, Shattuck MD, Snyder LE, Potter JD, McDowell WH (2017) Deconstructing the effects of flow on DOC, nitrate, and major ion interactions using a high-frequency aquatic sensor network. Water Resour Res 53:10655–10673. https://doi.org/10.1002/2017WR020739

Lal R, Delgado JA, Groffman PM, Millar N, Dell C, Rotz A (2011) Management to mitigate and adapt to climate change. J Soil Water Conserv 66:276–285. https://doi.org/10.2489/jswc.66.4.276

Larson J, Zhou Y, Higgins RW (2005) Characteristics of landfalling tropical cyclones in the United States and Mexico: climatology and interannual variability. J Clim 18:1247–1262. https://doi.org/10.1175/JCLI3317.1

Lavers DA, Villarini G (2013) Atmospheric rivers and flooding over the central United States. J Clim 26:7829–7836. https://doi.org/10.1175/JCLI-D-13-00212.1

Lavers DA, Villarini G, Allan RP, Wood EF, Wade AJ (2012) The detection of atmospheric rivers in atmospheric reanalyses and their links to British winter floods and the large-scale climatic circulation. J Geophys Res Atmos 117:1–13. https://doi.org/10.1029/2012JD018027

Lawrence JR, Gedzelman SD (1996) Low stable isotope ratios of tropical cyclone rains. Geophys Res Lett 23:527–530

Lee ES, Krothe NC (2001) A four-component mixing model for water in a karst terrain in south-central Indiana, USA. Using solute concentration and stable isotopes as tracers. Chem Geol 179:129–143. https://doi.org/10.1016/S0009-2541(01)00319-9

Luhmann AJ, Covington MD, Alexander SC, Chai SY, Schwartz BF, Groten JT, Alexander EC (2012) Comparing conservative and nonconservative tracers in karst and using them to estimate flow path geometry. J Hydrol 448–449:201–211. https://doi.org/10.1016/j.jhydrol.2012.04.044

Martin JB, Dean RW (2001) Exchange of water between conduits and matrix in the Floridan aquifer. Chem Geol 179:145–165. https://doi.org/10.1016/S0009-2541(01)00320-5

Mellander P-E, Melland AR, Jordan P, Wall DP, Murphy PNC, Shortle G (2012) Quantifying nutrient transfer pathways in agricultural catchments using high temporal resolution data. Environ Sci Policy 24:44–57

Miller MP, Tesoriero AJ, Hood K, Terziotti S, Wolock DM (2017) Estimating discharge and nonpoint source nitrate loading to streams from three end-member pathways using high-frequency water quality data. Water Resour Res 53:10201–10216. https://doi.org/10.1002/2017WR021654

Moatar F, Abbott BW, Minaudo C, Curie F, Pinay G (2017) Elemental properties, hydrology, and biology interact to shape concentration-discharge curves for carbon, nutrients, sediment, and major ions. Water Resour Res 53:1270–1287. https://doi.org/10.1002/2016WR019635

Molson J, Pehme P, Cherry J, Parker B (2007) Numerical analysis of heat transport within fractured sedimentary rock: implications for temperature probes. In: EPA Fractured rock conference: state of the science and measuring success in remediation (#5017). Portland, Maine

Moore BJ, Neiman PJ, Ralph FM, Barthold FE (2012) Physical processes associated with heavy flooding rainfall in Nashville, Tennessee, and Vicinity during 1–2 May 2010: the role of an atmospheric river and mesoscale convective systems. Mon Weather Rev 140:358–378. https://doi.org/10.1175/MWR-D-11-00126.1

NHC NOAA (National Hurricane Center) (2017) Hurricane NATE advisory archive. http://www.nhc.noaa.gov/archive/2017/NATE.shtml? Accessed 6 Nov 2017

NOAA (National Oceanic and Atmospheric Administration) (2017a) Billion-dollar weather and climate disasters: overview. http://www.ncdc.noaa.gov/billions. Accessed 6 May 2018

NOAA (National Oceanic and Atmospheric Administration) (2017b) Lexington Blue Grass Airport. http://w1.weather.gov/data/obhistory/KLEX.html. Accessed 1 Jan 2018

Padilla IY, Vesper D (2018) Fate, transport, and exposure of emerging and legacy contaminants in karst systems: state of knowledge and uncertainty. In: White WB, Herman JS, Herman EK, Rutigliano M (eds) Karst groundwater contamination and public health. Springer, Berlin, Germany, pp 33–49

Panno SV, Hackley KC, Hwang HH, Kelly WR (2001) Determination of the sources of nitrate contamination in karst springs using isotopic and chemical indicators. Chem Geol 179:113–128. https://doi.org/10.1016/S0009-2541(01)00318-7

Paylor R, Currens JC (2004) Royal springs karst groundwater travel time investigation. A report prepared for Georgetown Municipal Water and Sewer Service. Lexington, KY

Pellerin BA, Downing BD, Kendall C, Dahlgren RA, Kraus TEC, Saraceno J, Spencer RGM, Bergamaschi BA (2009) Assessing the sources and magnitude of diurnal nitrate variability in the San Joaquin River (California) with an in situ optical nitrate sensor and dual nitrate isotopes. Freshw Biol 54:376–387. https://doi.org/10.1111/j.1365-2427.2008.02111.x

Phillips JD (2015) Emergent ecosystem engineering in epikarst. https://geography.as.uky.edu/blogs/jdp/emergent-ecosystem-engineering-epikarst. Accessed 6 May 2018

Phillips JD, Martin LL, Nordberg VG, Andrews WA (2004) Divergent evolution in fluviokarst landscapes of central Kentucky. Earth Surf Process Landf 29:799–819. https://doi.org/10.1002/esp.1070

Ralph FM, Dettinger MD (2012) Historical and national perspectives on extreme west coast precipitation associated with atmospheric rivers during December 2010. Bull Am Meteorol Soc 93:783–790. https://doi.org/10.1175/BAMS-D-11-00188.1

Rusjan S, Brilly M, Mikoš M (2008) Flushing of nitrate from a forested watershed: an insight into hydrological nitrate mobilization mechanisms through seasonal high-frequency stream nitrate dynamics. J Hydrol 354:187–202. https://doi.org/10.1016/j.jhydrol.2008.03.009

Rutz JJ, Steenburgh WJ, Ralph FM (2014) Climatological characteristics of atmospheric rivers and their inland penetration over the Western United States. Mon Weather Rev 142:905–921. https://doi.org/10.1175/MWR-D-13-00168.1

Schilling KE, Helmers M (2008) Tile drainage as karst: conduit flow and diffuse flow in a tile-drained watershed. J Hydrol 349:291–301. https://doi.org/10.1016/j.jhydrol.2007.11.014

Shepherd JM, Grundstein A, Mote TL (2007) Quantifying the contribution of tropical cyclones to extreme rainfall along the coastal southeastern United States. Geophys Res Lett 34:1–5. https://doi.org/10.1029/2007GL031694

Sigman DM, Casciotti KL, Andreani M, Barford C, Galanter M, Böhlke JK (2001) A bacterial method for the nitrogen isotopic analysis of nitrate in seawater and freshwater. Anal Chem 73:4145–4153. https://doi.org/10.1021/ac010088e

Sinha E, Michalak AM (2016) Precipitation dominates interannual variability of riverine nitrogen loading across the continental United States. Environ Sci Technol 50:12874–12884. https://doi.org/10.1021/acs.est.6b04455

Spangler LE (1982) Karst hydrogeology of northern Fayette and southern Scott counties, Kentucky. Master's Thesis. University of Kentucky. Lexington, Kentucky

St-Jean G (2003) Automated quantitative and isotopic (13C) analysis of dissolved inorganic carbon and dissolved organic carbon

in continuous-flow using a total organic carbon analyser. Rapid Commun Mass Spectrom 17:419–428. https://doi.org/10.1002/rcm.926

Taylor CJ (1992) Ground-water occurrence and movement associated with sinkhole alignments in the Inner Bluegrass Karst region of central Kentucky. Master's Thesis. University of Kentucky. Lexington, Kentucky

Tesoriero AJ, Duff JH, Saad DA, Spahr NE, Wolock DM (2013) Vulnerability of streams to legacy nitrate sources. Environ Sci Technol 47:3623–3629. https://doi.org/10.1021/es305026x

Thrailkill J, Sullivan SB, Gouzie DR (1991) Flow parameters in a shallow conduit-flow carbonate aquifer, Inner Bluegrass Karst region, Kentucky, USA. J Hydrol 129:87–108. https://doi.org/10.1016/0022-1694(91)90046-K

Tomer MD, Schilling KE (2009) A simple approach to distinguish land-use and climate-change effects on watershed hydrology. J Hydrol 376:24–33. https://doi.org/10.1016/j.jhydrol.2009.07.029

Toran L, White WB (2005) Variation in nitrate and calcium as indicators of recharge pathways in Nolte Spring, PA. Environ Geol 48:854–860. https://doi.org/10.1007/s00254-005-0018-y

Tzoraki O, Nikolaidis NP (2007) A generalized framework for modeling the hydrologic and biogeochemical response of a Mediterranean temporary river basin. J Hydrol 346:112–121. https://doi.org/10.1016/j.jhydrol.2007.08.025

UKCAFE (University of Kentucky College of Agriculture, Food, and the Environment) (2011) Cane Run and Royal Spring watershed-based plan, version 5. EPA project number C9994861-06. http://www.bae.uky.edu/CaneRun/PDFs/Cane_Run_WBP _2011.pdf. Accessed 6 Jan 2018

USDA (United States Department of Agriculture) (1993) Soil survey manual. Handbook no. 18. United States Department of Agriculture, Washington DC, USA

Vesper DJ, White WB (2004) Storm pulse chemographs of saturation index and carbon dioxide pressure: implications for shifting recharge sources during storm events in the karst aquifer at Fort Campbell, Kentucky/Tennessee, USA. Hydrogeol J 12:135–143. https://doi.org/10.1007/s10040-003-0299-8

Williams PW (2008) The role of the epikarst in karst and cave hydrogeology: a review. Int J Speleol 37:1–10. https://doi.org/10.2307/2423146

Winston WE, Criss RE (2004) Dynamic hydrologic and geochemical response in a perennial karst spring. Water Resour Res 40:1–11. https://doi.org/10.1029/2004WR003054

Xue D, Botte J, De Baets B, Accoe F, Nestler A, Taylor P, Van Cleemput O, Berglund M, Boeckx P (2009) Present limitations and future prospects of stable isotope methods for nitrate source identification in surface- and groundwater. Water Res 43:1159–1170. https://doi.org/10.1016/j.watres.2008.12.048

Yue F-J, Li S-L, Zhong J, Liu J (2018) Evaluation of factors driving seasonal nitrate variations in surface and underground systems of a karst catchment. Vadose Zo J 17:1–10. https://doi.org/10.2136/vzj2017.04.0071

Zhu J, Currens JC, Dinger JS (2011) Challenges of using electrical resistivity method to locate karst conduits—a field case in the Inner Bluegrass region, Kentucky. J Appl Geophys 75:523–530. https://doi.org/10.1016/j.jappgeo.2011.08.009